Theory of action potentials

Romain Brette

April 5, 2018

Contents

Chapter 6

Spike initiation with an initial segment

6.1 The spike initiation system of neurons

6.1.1 Axonal spike initiation

We have started to study excitability on isopotential models (chapter **??**), where it is assumed that the membrane potential is identical everywhere in the cell. This corresponds to the space-clamp configuration studied by Hodgkin and Huxley in the squid giant axon, where the axon's intracellular medium is made isopotential by inserting a metal wire inside it. Indeed most classical theoretical work on excitability (but obviously, not on conduction) addresses this particular configuration. It should be reminded that the Hodgkin-Huxley is not (and has never been) a model of spike initiation in neurons. It was developed to investigate the biophysical basis of excitability, which turned out to be quite universal across all kingdoms of life, with variations on the nature of the ions involved and the properties of ionic channels (section **??**). The model explains how a piece of membrane can be excited, and how an axon propagates spikes. But it does not explain how a spike is normally initiated in a neuron, which has a spatially extended structure. In fact, as already mentioned, the squid giant axon is a rather peculiar axon in that it results from the fusion of hundreds of cells, a syncytium (Young, 1936).

Early work on vertebrate motoneurons showed that spikes recorded in the soma have two distinct components (Coombs et al., 1957b; Fatt, 1957). Figure 6.1A shows somatic spikes elicited by three different means. The first one is obtained by stimulating the axon and is called *antidromic* spike. The second one is obtained by stimulating a synaptic afferent, and the third one is obtained by stimulating the soma with a current injection. These latter two spikes are called *orthodromic* spikes. The term orthodromic refers to the direction of propagation that normally occurs *in vivo*: synaptic currents coming from the dendrites are collected at the soma, and therefore the primary source of excitation is in the soma or somatodendritic compartment, not in the axon, in contrast with the antidromic spike.

In these three cases, one can distinguish two components in the somatic

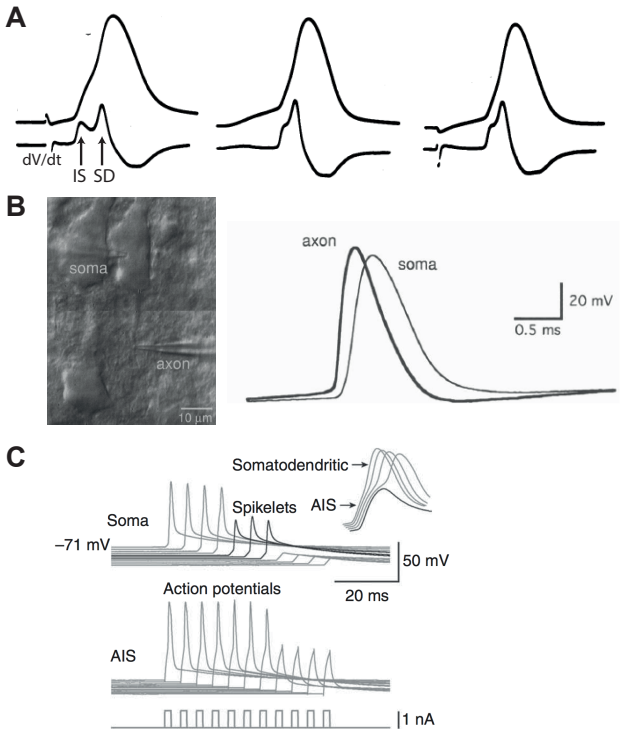

Figure 6.1: Axonal spike initiation in neurons. A, Action potential elicited by three different means and recorded in the soma of a motoneuron with a microelectrode (Coombs et al., 1957b). Left: exciting the axon; middle: exciting synaptic afferents; right: injecting a current in the soma. The bottom curve shows the derivative of the membrane potential, where two distinct components are seen. B, Simultaneous recording of an action potential in the soma and axon (23 μm from the soma) of a pyramidal cortical neuron, with current injection in the soma (Stuart et al., 1997). C, Simultaneous recording in the soma and axon of a pyramidal cortical neuron of spikes elicited by current injection in the axon, where the soma is hyperpolarized at different values (Hu et al., 2009).

action potential, which are more clearly seen in the derivative dV/dt of the membrane potential (Fig. 6.1A, bottom). It has been shown that the first component originates from a short segment of axon next to the soma called the *axon initial segment* (AIS), while the second originates from the soma and proximal dendrites. For this reason, these two components have been termed initial segment (IS) and somatodendritic (SD) components in the literature. These components can be separated: for example, the SD component can be blocked by hyperpolarizing the soma; the IS component can be blocked by applying TTX on the AIS (Palmer and Stuart, 2006; Kole and Stuart, 2008).

The IS component, coming from the axon, always arises before the SD component, even when the stimulation comes from the soma or dendrites. This finding has been confirmed in more recent studies in pyramidal cortical neurons by direct patch-clamp recordings in the soma and axon (Fig. 6.1B) (Debanne

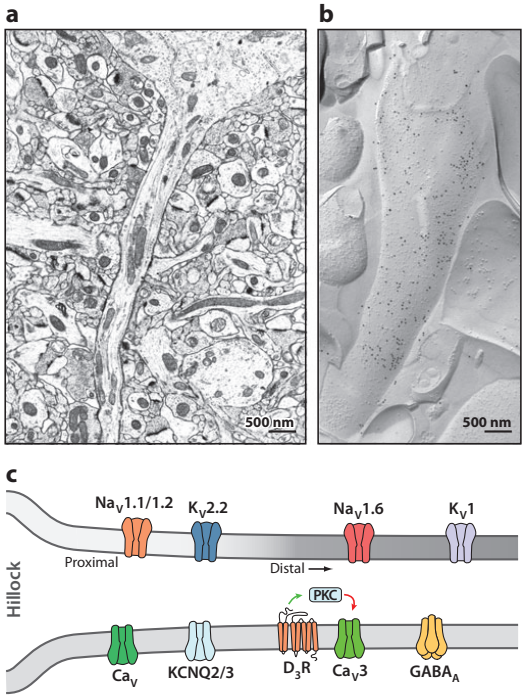

Figure 6.2: Structure of the axon initial segment (from Bender and Trussell (2012)). A, Electron micrograph of the AIS of a cortical pyramidal neuron. B, Freeze-fracture immunogold labeling of Nav1.6 channels in a hippocampal pyramidal cell. C, Ion channels and receptors found in the AIS.

et al., 2011): an action potential can be measured first in the axon, a few tens of μm away from the soma, before it is observed in the soma (Palmer and Stuart, 2006; Stuart et al., 1997). Spikes elicited by current injection in the AIS can be observed in the soma, but if the soma is hyperpolarized, a smaller all-or-none spike is seen (a *spikelet*), which reflects the axonal spike (Fig. 6.1C).

Also loose patch and voltage imaging

6.1.2 The axon initial segment

On the basis of extracellular recordings and voltage imaging, recent work has shown that the site of spike initiation is typically located 15-40 μm away from the soma, at the distal end of a highly organized molecular structure, the axon initial segment (Bender and Trussell, 2012). This is a structure of a few tens of micrometer next to the cell body packed with ionic channels, in particular sodium channels (Figure 6.2). These channels are attached to the cytoskeleton by a scaffold protein called ankyrin-G, which is specific of the AIS.

The AIS has two distinct roles in the cell. One is to maintain neuronal polarity by regulating intracellular traffic, filtering proteins targeted to the axon from those targeted to the soma and dendrites. It also prevents the diffusion of somatodendritic membrane proteins to axon (Leterrier and Dargent, 2014). Another role is the initiation of spikes.

Why do spikes initiate in the AIS?

If a homogeneous axon is excited by injecting current at one point, an action potential initiates at that point, in the sense that a regenerative Na^+ current first enters the membrane around that point. This is so because the current injection produces a local depolarization that attenuates with distance, and therefore more Na^+ channels open near the stimulation point. The same would be true if a neuron with homogeneous membrane (homogeneous channel densities) but complex geometry were excited with a local current injection (e.g. a synaptic current): the action potential would initiate from wherever the neuron is stimulated.

It has been proposed that spikes initiate in the AIS because less current is necessary to produce a spike in the AIS than in the soma (Kole and Stuart, 2008). In other words, the initiation site is the point of lowest local threshold current (*rheobase*). This argument is invalid. In a neuron with a complex structure (soma, dendrites and axon) but homogeneous conductance densities, initiation always occurs at the point of stimulation. Yet, the input resistance differs between different points in the neuron depending on local geometry, and therefore so does the local rheobase. For example, as we have seen in section **??**, the input resistance in the middle of an axon is:

$$R_a = \frac{1}{\pi}\sqrt{r_m R_i} d_a^{-3/2}$$

where d_a is axon diameter. In contrast, the input resistance in a somatic sphere (neglecting the contribution of dendrites and axon[1]) is

$$R_s = \frac{r_m}{\pi d_s^2}$$

where d_s is somatic diameter. Let us choose for example $d_s = 40$ μm, $d_a = 1$ μm, $r_m = 15000$ Ω.cm^2 and $R_i = 100$ Ω.cm. We find $R_a \approx 390$ MΩ and $R_s \approx 290$ MΩ. The input resistance is larger in the axon, and therefore the rheobase is lower (assuming identical conductance densities). Yet the action potential would still initiate in the soma when current is injected in the soma.

The spike initiation site can only differ from the stimulation site if conductance densities are not homogeneous. Let us consider a current injection in the soma, which also depolarizes nearby sites, in particular the AIS. For a long current step, the membrane potential will be similar in the soma and AIS, if we consider only passive properties. As we have seen in section **??**, below the half-activation voltage of Na^+ channels, the Na^+ current density at a given point on the membrane is an approximately exponential function of voltage:

$$I_{Na} \approx g_{Na} \exp\Big(\frac{V - V_{1/2}}{k}\Big)(E_{Na} - V)$$

where g_{Na} is the conductance density of Na^+ channels and $V_{1/2}$ is their half-activation voltage[2]. We can see in this formula that more current can be produced locally if there is a higher density of Na^+ channels (larger g_{Na}) or if the

[1] This contribution would reduce the input resistance, and therefore only strengthen the point being made here. In fact, one can calculate the input resistance at the soma for a sphere connected to a semi-infinite cylindrical axon by adding the conductances of the two pieces, which with our notations gives a resistance of $(2R_a^{-1} + R_s^{-1})^{-1} \approx 118$ MΩ.

[2] Here we have used the linear (ohmic) model of currents, but the same conclusion would follow with the GHK model.

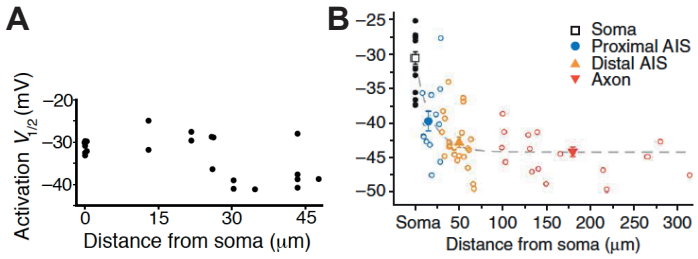

Figure 6.3: Variation of half-activation voltage of Na^+ channels along the axon, as a function of distance from the soma (A, Colbert and Pan (2002); B, Hu et al. (2009)).

half-activation voltage $V_{1/2}$ is lower. If we define the spike initiation site as the point where the initial Na^+ current density is highest and we assume that k is constant, then this site is determined by the minimum of the following voltage:

$$V_{1/2} - k \log g_{Na}$$

We note the relation with the threshold equation (section **??**). There is empirical evidence that both $V_{1/2}$ and g_{Na} make this voltage lower at the AIS.

In layer 5 pyramidal neurons, $V_{1/2}$ is indeed 7-14 mV lower in the distal AIS than in the soma, and decreases with increasing distance from the soma (Colbert and Pan, 2002; Hu et al., 2009) (Fig. 6.3). This could be due to spatial inhomogeneities in the distribution of Na^+ channels subtypes, with Nav1.2 channels at the proximal end and Nav1.6 channels at the distal end of the AIS, Nav1.6 channels having a lower half-activation voltage (Rush et al., 2005). It might also be due to spatial inhomogeneities in channel phosphorylation, as has been observed for K^+ channels (Misonou et al., 2004).

The measurements of Na^+ channel densities are more contentious but lean towards a higher density in the AIS than in the soma. Immunostaining of Na^+ channels consistently indicates higher channel density in the AIS of various neuron types (Meeks and Mennerick, 2007; Wollner and Catterall, 1986; Boiko et al., 2003; Van Wart et al., 2007; Inda et al., 2006) (Fig. 6.4A). There are two potential issues with immunostaining: 1) the fluorescent signal allows relative but not absolute estimates of channel density, and 2) antibodies mark not only functional channels present at the membrane, but also channels in the cytoplasm and non-functional channels. To address these two issues, one can use electron microscopy with the freeze-fracture method. Electron microscopy has a higher resolution than optical microscopy, precise enough to allow counting individual channels. Freeze-fracture allows labeling channels that are specifically inserted in the membrane. By this technique, Lorincz and Nusser (2010) counted around 200 Nav1.6 channels per μm^2 in the AIS of hippocampal pyramidal cells (Fig. 6.4B). Given that the conductance of a single Nav channel is about 15 pS (Colbert and Johnston, 1996), this makes a conductance density of about $g_{Na} \approx 3000$ pS/μm^2, assuming all channels are functional. Electrophysiological measurements indicate that Na^+ conductance density is about 40-60 pS/μm^2 in the soma and dendrites (Stuart and Sakmann, 1994; Magee and Johnston, 1995).

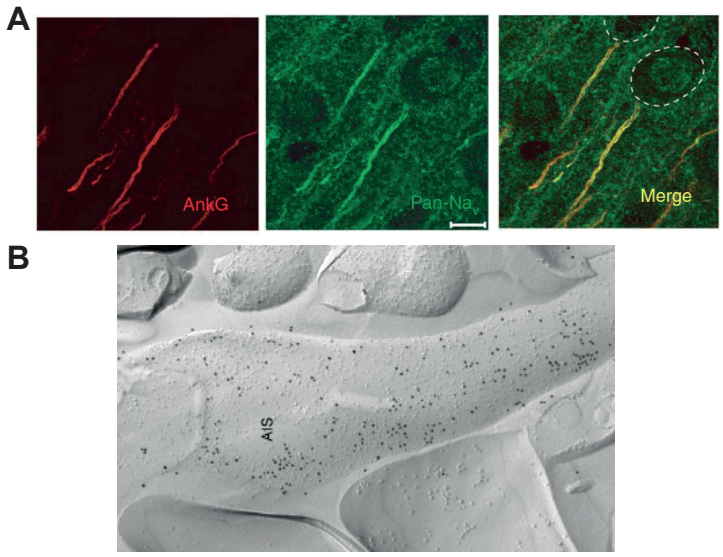

Figure 6.4: Density of Na^+ channels in the AIS marked by immunostaining. A, Immunostaining of ankyrin-G, a structural marker of the AIS (left), Na^+ channels (middle) and merged picture with the soma shown with a dashed curve (right) (Hu et al., 2009). B, Individual Na^+ channels (dots) on the AIS membrane, revealed using the electron microscopic immunogold technique (Lorincz and Nusser, 2010).

Thus it is clear that there is a much higher density of Na^+ channels in the AIS than in the soma and dendrites. However, electrophysiological measurements of conductance density in the AIS found similar values to the somatic density, corresponding to about 3-4 functional channels per μm^2 (Colbert and Johnston, 1996; Colbert and Pan, 2002). Thus, one interpretation is that many of those channels are indeed not functional. However, a plausible explanation for the discrepancy is that Nav channels are attached to the cytoskeleton (via Ankyrin-G), so when Na^+ currents are measured in patch-clamp, the channels do not remain on the patch membrane but instead remain attached to the cytoskeleton. Consistent with this hypothesis, disrupting the cytoskeleton with an enzyme increases the measured currents several fold (Kole et al., 2008).

There are some subtleties in the notion of spike initiation site. We have defined it above as the point where Na^+ current first enters the membrane when a spike is initiated. This point does not exactly match the point where the membrane potential increases most rapidly, which can be further away from the soma (Baranauskas and Martina, 2006). The reason is the resistive coupling between the soma and AIS, which we will study further in sections 6.1.4, 6.2 and 6.3.

Finally, there is another hypothesis to explain why spikes initiate in the AIS, but one for which there is no experimental evidence. Classically, it is assumed that the opening of a channel does not influence the opening of neighboring channels. If, for example by mechanical interactions through the cytoskeleton, the opening of a Na^+ channel in the AIS increased the probability that a neigh-

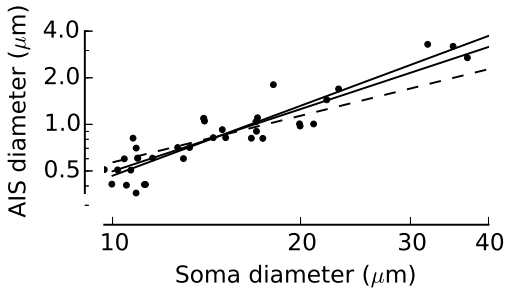

Figure 6.5: Relation between AIS diameter and somatic diameter for cortical neurons of different types, shown in log-log scale (adapted from Sloper and Powell (1979)). The two solid lines are the best power-law fits with exponents 3/2 and 4/3 (mean square error in log-log space); the dashed line is the best fit with exponent 1 (i.e., linear relation).

boring channel opens, then the population of channels would open on average at a lower voltage than if they did not interact. This is called the *cooperativity hypothesis*, which we will discuss further in section 6.1.5.

Organization of the AIS

TO DO

6.1.3 Geometry of the spike initiation system

Dimensions of the soma and axon

A striking geometrical feature of the spike initiation system of neurons is that the soma is 1-2 orders of magnitude larger than the proximal axon where the AIS is located. Figure 6.5 shows AIS vs. somatic diameter for cortical neurons of different types (Sloper and Powell, 1979). The relation is not linear; the data are better fitted by a power law function: $d_{\text{AIS}} \propto d_{\text{soma}}^{\alpha}$, with exponent 1.42 ± 0.1 (mean $\pm$ standard deviation from a bootstrap analysis, using a linear regression in log-log space). In the cerebellum, granule cells have a very small soma of about 6 μm (Diwakar et al., 2009), and the proximal axon is correspondingly small, with a diameter of about 0.2 - 0.3 μm (Perge et al., 2012; Wyatt et al., 2005).

Can we explain this scaling relationship? We will discuss two theoretical ideas. The first one is based on molecular transport. Transcription, the production of mRNA from DNA, occurs in the cell body. Let us assume that the rate of production in the cell body is proportional to its volume, which scales as d_{soma}^3. The mRNA molecules are then transported to target locations, including the axon. To simplify, let us assume that all the molecules produced go to the axon. The maximum flux of proteins through the axon is proportional to the axon's section, which scales as d_{AIS}^2. For the flux through the axon to match the production rate in the cell body, AIS diameter must then scale as $d_{\text{AIS}} \propto d_{\text{soma}}^{3/2}$. Of course, we have neglected an important element, which is the

This idea of molecular transport should apply to the more distal axon actually, say before the first branching.

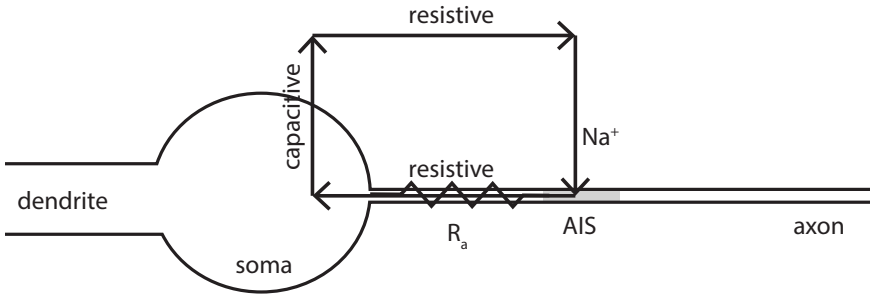

Figure 6.6: Circulation of current at spike initiation in resistive coupling theory. The soma and AIS are coupled by axial resistance R_a.

transport of proteins to the dendrites. Nonetheless, we obtain an exponent that is compatible with the empirical data shown in Fig. 6.5.

The second idea is to compare the capacitances of the soma and proximal axon. The capacitance of the soma is proportional to d^2_{soma}. The capacitance of a characteristic length of axon scales as $d^{3/2}_{\text{AIS}}$ (see chapter **??**). For these two capacitances to scale similarly with cell size, the following scaling relation must hold: $d_{\text{AIS}} \propto d^{4/3}_{\text{soma}}$. Again, we have neglected the contribution of the dendrites to the somatodendritic capacitance. This exponent is also compatible with the data in Fig. 6.5.

Regardless of the explanation for this scaling relation, the soma is consistently much larger than the proximal axon where the AIS is located.

AIS geometry

TODO

6.1.4 Resistive coupling theory

The resistive coupling theory (Brette, 2013, 2015; Telenczuk et al., 2017) of spike initiation is based on a simplified model consisting of two points coupled by a resistance: an excitable "hotspot", the AIS, and a passive somatodendritic compartment. This model is proposed to capture the main features of the spike initiation system. The theory describes the circulation of current at spike initiation as follows (see Fig. 6.6):

Actually, we implicitly assumed the same extracellular potential near soma and AIS

1. At spike initiation, Na^+ current first enters the membrane at the AIS. As we have seen previously, this occurs because of higher local density of Na^+ channels and/or of lower half-activation voltage.

2. This current flows mostly towards the soma. This is because the distal end of the AIS is charged very rapidly owing to the relatively small size of the axon, so the current mainly charges the soma except for a very transient time. The soma is said to be a *current sink* for the axonal initiation site,

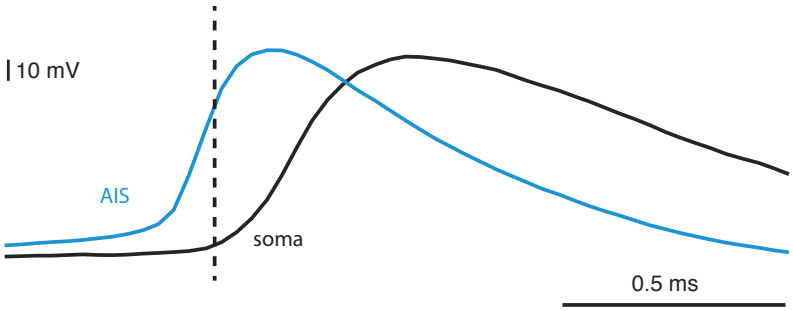

Figure 6.7: Time course of the somatic and AIS spikes in cortical pyramidal neurons (adapted from Kole and Stuart (2008)). At spike initiation, the somatic potential barely increases while the AIS potential rises.

which is a *current source*. For the same reason, this current is mainly resistive (the axonal capacitive current is transient and small).

3. The current escapes the membrane at the somatodendritic compartment as capacitive current. Because of the large size of the soma, the somatic potential increases slowly compared to the axonal potential.

4. The current loop is closed by an extracellular current returning to the initiation site.

Here the axon is viewed as a simple resistor, with channels on a "hotspot". Axonal capacitance and leak are neglected. Because of the geometric discontinuity between the soma and axon, there is a separation of timescales: the axonal potential increases very quickly (here, it is assumed to be instantaneous) compared to the somatic membrane potential. In effect, the soma essentially "clamps" the beginning of the axon during the rising phase of the spike (Fig. 6.7). The theory predicts that when the Na^+ conductance is large enough compared to the axial conductance (between soma and initiation site), an all-or-none spike is produced in the AIS when the somatic voltage reaches a threshold — otherwise the increase is gradual. The theory has a few important implications:

1. Somatic voltage is the main variable determining the condition for spiking, in contrast with the isopotential case, where a threshold can only be defined on a stimulus parameter (section 6.2.4). In terms of modeling, a counterintuitive implication is that the response of a neuron to somatic stimulation is more accurately modeled by an integrate-and-fire model than by an isopotential Hodgkin-Huxley model (Brette, 2015).

2. Excitability and backpropagated current depend on the geometry and position of the AIS.

3. Channels at the AIS can strongly impact excitability with little impact on the somatic membrane potential.

First, we will examine the first part of the current circulation diagram: the Na^+ current matches the axial resistive current (section 6.2). This identity determines the conditions of spike initiation. Second, we will examine the second

part of the current circulation diagram: the axial resistive current matches the somatodendritic capacitive current (section 6.3). This identity determines the conditions of spike transmission to the soma. Before we study resistive coupling theory in detail, we describe an alternative theory based on cooperative opening of Na^+ channels.

6.1.5 Cooperative opening of Na^+ channels

Maybe this should be at the end or in an appendix

Theory of cooperative spike initiation

We have seen in section 6.1.2 that the fact that spikes initiate in the AIS could be due to higher local Na^+ channel density, hyperpolarized voltage-dependence (lower half-activation voltage) or a combination of the two. An alternative possibility is that Na^+ channels in the AIS *cooperate*. This hypothesis was first introduced by Naundorf et al. (2006) to explain the fact that the onset of spikes recorded at the soma of cortical neurons appears very sharp, with a distinct kink, as if Na^+ channels opened as a step function of somatic membrane potential (see also Brette (2015)). We will see in section 6.2.3 that this phenomenon can also be explained by resistive coupling theory.

Channel cooperativity is the idea that the probability that a channel opens depends on the state of neighboring channels. This phenomenon has been observed in calcium (Marx et al., 1998, 2001), potassium (Molina et al., 2006; Kim et al., 2014) and HCN channels (Dekker and Yellen, 2006), in pharmacologically altered Na channels of cardiac myocytes (Undrovinas et al., 1992). In the case of Na^+ channels in the AIS, we could imagine for example that the anchoring to the cytoskeleton might introduce mechanical interactions between channels. Classical channel theory considers that the opening of individual channels is all-or-none but stochastic and independent between channels. This independence implies that macroscopically, the current produced by a population of voltage-dependent channels varies gradually with membrane potential, mirroring the activation probability function of individual channels. This is no longer the case if channels cooperate.

Specifically, let $m(V)$ be the activation curve, i.e., the steady-state probability that a channel is open when the membrane potential is V, in the absence of interactions. Let x be the macroscopic proportion of open channels. Without interactions, $x = m(V)$. We model cooperativity by postulating that each open channel hyperpolarizes the activation curve of other channels by some fixed amount. This amounts to postulating that

$$x = m(V + Jx)$$

where $J > 0$ is a coupling parameter representing the strength of interactions. The first consequence is that channels tend to open at lower voltage. Let us calculate the half-activation voltage $V^*_{1/2}$, that is, the value of V when $x = 1/2$:

$$\frac{1}{2} = m\Big(V^*_{1/2} + \frac{J}{2}\Big)$$

If $V_{1/2}$ is the half-activation voltage in the absence of interactions ($J = 0$), then we have:

$$V^*_{1/2} = V_{1/2} - \frac{J}{2}$$

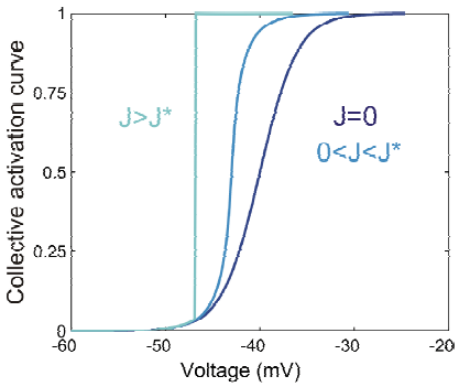

Figure 6.8: Macroscopic activation curve $x(V)$ of cooperative channels for different values of the coupling parameter J (from Naundorf et al. (2006)). The curve becomes discontinuous when J is greater than the critical value J^*.

Thus the half-activation voltage is hyperpolarized in proportion of the coupling parameter. This could explain that spikes initiate in the AIS, even if the density and properties of channels were the same as in the soma.

A second consequence of cooperative opening is that the macroscopic activation curve becomes steeper[3] (Fig. 6.8). In fact, if J is large enough, the activation curve $x(V)$ becomes discontinuous: when V exceeds a certain value, x increases abruptly, i.e., most channels open simultaneously. This can be seen by plotting the two curves $y = x$ and $y = m(V + Jx)$ for a given V (see Fig. 6.9). The value of $x(V)$ is given by the intersection of the two curves. Changing V amounts to shifting the sigmoidal curve. At some point when V is increased from a low value, the lower intersection point disappears and therefore m jumps to the higher intersection point: this is a bifurcation. As we have seen before, the bifurcation point can be calculated by differentiating the fixed point equation with respect to the variable x:

$$1 = Jm'$$

where the argument of m' has been omitted. If m is a Boltzmann function of slope k, we then have:

$$\begin{aligned} Jm(1-m) &= k \\ x &= m \end{aligned}$$

It follows that x is the solution of a quadratic equation:

$$x = \frac{1}{2}\left(1 - \sqrt{1 - 4k/J}\right)$$

where we indicate the lower solution. We can see that this bifurcation occurs if $J > 4k$. Thus there is a critical value $J^* = 4k$ (about 24 mV, with $k = 6$ mV) for the coupling parameter, above which channels open abruptly.

[3]This can be seen by differentiating with respect to V, which leads to $x' = m'/(1 - Jm')$, where the argument of m' has been omitted. The denominator makes the derivative of the macroscopic activation function $x(V)$ steeper than the microscopic activation function $m(V)$.

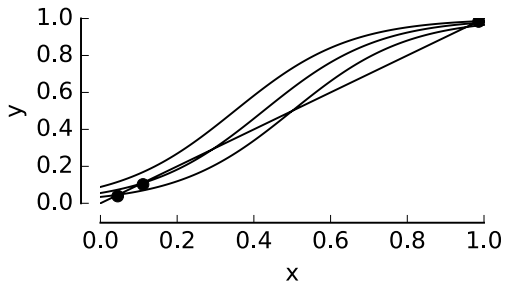

Figure 6.9: Bifurcation in cooperative opening. The diagonal $y = x$ is plotted with the sigmoidal curves $y = m(V + Jx)$ for $V = -50$, -47 and -44 mV, where $J = 40$ mV, $k = 6$ mV and $V_{1/2} = -30$ mV. The proportion of open channels $x(V)$ is the lower intersection of the two curves (dots). When V exceeds a threshold, $x(V)$ suddenly jumps to a value near 1.

When this bifurcation occurs, we can calculate the threshold value V^* by inverting m:

$$\begin{aligned} V^* &= m^{-1}(x) - Jx \\ &= V_{1/2} - k \log\left(\frac{1}{x} - 1\right) - Jx \end{aligned}$$

where x is given by the formula above. At critical coupling ($J = J^*$), we get:

$$V^* = V_{1/2} - 2k$$

and increasing J lowers this value.

Experimental evidence

Although there is evidence of cooperativity in various channels and locations, current experimental evidence does not support this hypothesis for the Na^+ channels of the axon initial segment (AIS).

Patch-clamp recordings in the AIS of cortical neurons reveal spikes with a smooth onset (Kole et al., 2008; Kole and Stuart, 2008), which is not consistent with cooperative opening of Na^+ channels (z et al., 2015). The smoothness of the spike onset has been quantified in axonal blebs near the AIS, which are swellings formed on the axon by the slicing procedure, making the axon easier to access with an electrode (Yu et al., 2008). It appears that the smoothness is consistent with independent opening of Na^+ channels. It is unlikely that the failure to observe channel cooperativity is due to the disruption of the cytoskeleton by the experimental procedure. Channel cooperativity was meant to explain the fact that spikes recorded at the soma have a sharp onset, as if channels opened simultaneously (Naundorf et al., 2006), but these axonal recordings showing a smooth onset were performed simultaneously with somatic recordings, which showed spikes with a sharp onset. As we will see in section 6.2, this sharp onset at the soma can be explained by resistive coupling theory.

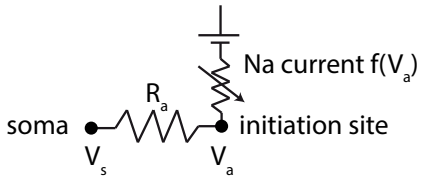

Figure 6.10: Resistive coupling model (adapted from Brette (2013)), with two sites (soma with potential V_s and initiation site with potential V_a) connected by axial resistance R_a.

6.1.6 Spike initiation in invertebrate neurons

TODO

6.2 Resistive coupling theory: spike initiation

6.2.1 The resistive coupling model

In its simplest version, the resistive coupling model consists of just two points, the soma and the axonal initiation site, coupled by a resistance (Fig. 6.10), with a voltage-dependent Na^+ current at the initiation site. This is a highly simplified model, which makes a number of assumptions and approximations. We now review the biophysical arguments and the experimental evidence.

In reality all this argumentation could and perhaps should apply to the circuit loop diagram, which summarizes the theory

Separation of somatic and axonal time scales

First, the model ignores all the somatic currents (capacitance, ionic channels, dendritic currents). This is because the somatic potential V_s is assumed to be constant at the time scale of interest. The reasoning behind this assumption is as follows.

The Na^+ current first increases in the AIS, not at the soma. As discussed in section 6.1.2, there is much experimental evidence for this fact, although there is ongoing discussion about its main cause (high channel density, lower activation voltage, cooperativity).

Because the soma is much larger than the beginning of the axon (see section 6.1.3), this current will charge the AIS much faster than the soma, so that the potential will first increase in the AIS while it increases only slightly in the soma. This point can be made theoretically with a simple calculation. The capacitance of a cortical layer 5 pyramidal cell measured at the soma is on the order of 300 pF (Arsiero et al., 2007). The capacitance of a characteristic length λ of axon is $\pi d \lambda c_m$, where d is axon diameter and c_m is specific membrane capacitance. With $d = 1$ μm , $\lambda = 500$ μm and $c_m = 1$ μF/cm^2, we obtain about 15 pF. Thus the somatodendritic capacitance (soma plus proximal dendrites) is more than an order of magnitude larger than the axonal capacitance. Patch-clamp recordings in the soma of cortical pyramidal cells show that the initial speed of rise (first peak of dV/dt, corresponding to the initial segment current) is about 250 V/s, while the maximum speed of rise in the AIS (or axonal bleb) is about

Figure 6.11: Stationary potential $V(x)$ along an axon clamped at the somatic end, with a current I injected at distance 20 μm (left) and 40 μm (adapted from Brette (2013)). The depolarisation is proportional to the axial resistance R_a between the soma and injection site.

1500 V/s (Yu et al., 2008), which might be an underestimation due to low-pass filtering by the electrode.

In effect, we consider that the soma clamps the potential at the beginning of the axon. This is shown empirically in simultaneous recordings of AIS and somatic potential at spike initiation (Fig. 6.7 adapted from Kole and Stuart (2008)). Another piece of evidence is that, when the soma is hyperpolarized in current clamp (i.e., it is not clamped by the electrode) and the AIS is simultaneously stimulated with short current pulses, then the spike onset at the soma is essentially the initial somatic voltage[4] (Hu et al., 2009). Similarly, some cortical neurons have an axon stemming from a dendrite, and when triggering a spike by stimulating the axon-carrying dendrite, the somatic spike onset is much lower than when triggering a spike from the soma (Thome et al., 2014). All these observations are consistent with the idea that the soma clamps the beginning of the axon at spike initiation.

The soma as a current sink for the initiation site

Second, the resistive model ignores the currents towards the distal side of the axon, as well as the membrane currents between the soma and initiation site (leak and capacitance), and considers that the current flowing towards the soma is essentially equal to the Na^+ current entering the initiation site. We say that the soma is a "current sink", i.e., all the current flowing into the AIS then flows towards the soma. This is an approximation that stems from the geometry of the system, which can be understood with elementary considerations from cable theory (see chapter **??**).

Consider a constant current I injected at a distance x from the soma, with the soma clamping the potential of the beginning of a cylindrical axon at V_s (Fig. 6.11). The input resistance towards the distal side of the axon is $R_{\text{distal}} = r_a\lambda$, where r_a is the axial resistance per unit length and λ is the characteristic length of the axon. The input resistance towards the proximal side of the axon can be

[4]The authors attributed this observation to spike threshold adaptation, but this is unlikely, because there is essentially no difference between measured spike onset and somatic voltage, and there is neither Na^+ channel inactivation nor Kv1 channel activation in the hyperpolarized range tested in that study.

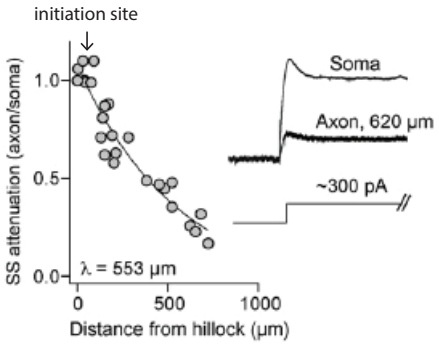

Figure 6.12: Voltage attenuation along a layer 5 cortical pyramidal cell axon, where the arrow show the position of the axonal initiation site (adapted from Kole et al. (2007)).

calculated[5] as in section **??**:

$$R_{\text{proximal}} = r_a \lambda \tanh \frac{x}{\lambda}$$

In cortical pyramidal cells, $\lambda \approx 500$ μm (Kole et al., 2007) (Fig. 6.12), while the axonal initiation site is a few tens of μm from the soma, on the order of 50 μm. Therefore, $R_{\text{proximal}} \approx r_a x$ and $R_{\text{distal}} \approx 10.R_{\text{proximal}}$. This means that about 90% of the current flows towards the soma: the soma is a *current sink* from the initiation site. This has been empirically shown in cortical pyramidal cells, where a current pulse is injected either at the soma or at the proximal axon (**?**). If all current flows towards the soma, then the same depolarization should be seen if the current is injected at the soma or at the (proximal) axon. This is shown on Fig. 6.13A for an axonal site at 180 μm (which is quite far compared to the AIS).

In terms of potential, the current sink hypothesis means that the current injection induces an essentially linear depolarization of the axon between the soma and the injection site (Fig. 6.11), of an amount approximately equal to $R_a I$, where R_a is the axial coupling resistance between the two sites, $R_a = r_a x$. In other words, on a short time scale, the input resistance at a point on the axon depends linearly on the distance to the soma (on a longer time scale, the input resistance at the soma must be added). This is shown empirically in Fig. 6.13B on axons of cortical pyramidal cells.

This shows in particular that the position of the initiation site has a large electrical impact. The stationary potential on the distal side of the axon is an exponential function of distance with characteristic length λ, which on the spatial scale of the AIS is nearly constant.

A qualification is that we have considered a constant current, while input resistances are frequency-dependent. At higher frequency, a larger proportion of the current charges the axon. This is expected to play a role mostly in the rising phase of the axonal spike, rather than at spike initiation or near the axonal peak.

[5] using the boundary conditions the *killed end* condition $V(0) = 0$ (taking V_s as the reference potential) and $V'(d) = r_a I$.

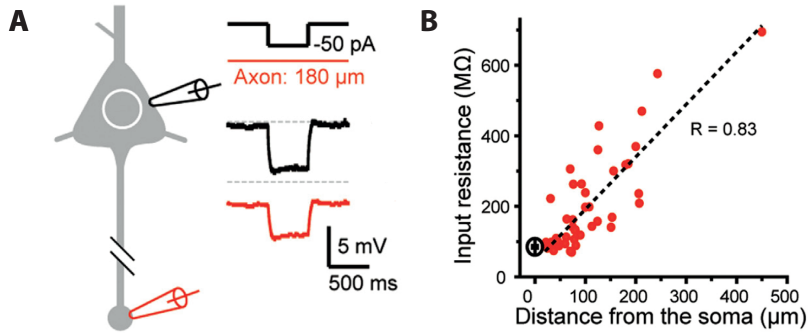

Figure 6.13: Experimental evidence that the soma acts as a current sink for the proximal axon (adapted from **?**). A, A current pulse injected at the axon, 180 μm away from the soma, produces a similar effect on the soma (red) as when it is injected directly into the soma (black). B, The input resistance measured at the axon scales linearly with the distance from the soma.

We can give an estimation of the different currents in the system at spike initiation. Considering a membrane surface between the soma and initiation site of about $S = 150$ μm^2 (corresponding to a distance of 50 μm and a diameter of 1 μm), the total capacitive current on that surface when the axonal potential increases at a speed of 20 V/s (already well above spike initiation) should not exceed 30 pA (using $c_m = 1$ μF/cm^2). With a specific membrane resistance of 15 000 Ω.cm^2, the total leak current over that surface would be about 10 pA for a 100 mV driving force (again well above spike initiation). In contrast, the resistive axial current should be $\Delta V/R_a$, where ΔV is the voltage difference between soma and initiation site. At spike initiation, this difference is empirically about 7 mV in cortical pyramidal cells (Kole and Stuart, 2008; Yu et al., 2008). As we will see in section 6.2.3, this is very close to theoretical prediction of the resistive model, which is $k_a \approx 6$ mV. The axial resistance is

$$R_a = \frac{4R_i}{\pi d^2}x$$

where R_i is intracellular resistivity. With $x = 40$ μm, $d = 1.5$ μm and $R_i = 150$ Ω.cm, we obtain $R_a \approx 34$ MΩ. It follows that the axial resistive current at spike initiation should be of order 200 pA. Thus, these estimations point to the axial resistive current being an order of magnitude larger than the capacitive and leak currents.

Our estimate for the axial current is strikingly similar to measurements of the persistent current at the soma of cortical pyramidal cells, which has been shown to originate from a Na^+ current in the AIS (Astman et al., 2006). At voltages near spike initiation, this current is of order 200 pA and is abolished by Na^+ channel blocker TTX (Fig. 6.14A). Similarly, the 7 mV voltage difference at spike initiation between the soma and initiation site disappears when TTX is applied (Fig. 6.14B,C). All these elements are consistent with the notion that at spike initiation, the axial current entering the soma is mostly resistive, with small contributions from passive transmembrane axonal currents, so that it matches the Na^+ current entering the initiation site.

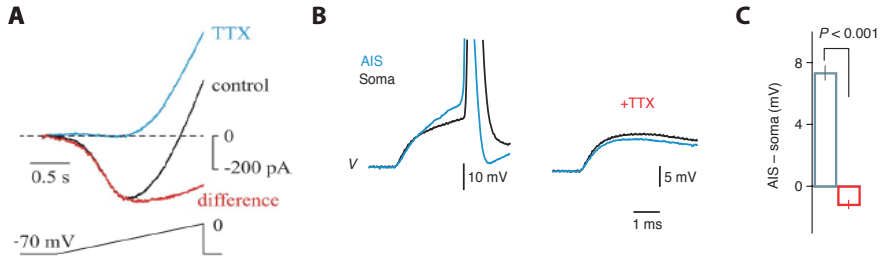

Figure 6.14: Axonal Na^+ current at spike initiation in pyramical cortical cells. A, Persistent Na^+ current recorded at the soma with a ramp of somatic voltage, in red (Astman et al., 2006). B, Membrane potential at the AIS and soma in response to current injection at the soma, without (left) and with (right) TTX (Kole and Stuart, 2008). C, Voltage difference between the two sites at spike initiation.

6.2.2 The equivalent isopotential model

Here we will expose a trick that allows reusing all the results from isopotential models (see chapter **??**) for the resistive coupling model. The electrical circuit shown in Fig. 6.15A resembles the equivalent circuit of an isopotential model, where V_a is identified to the membrane potential and the axial resistive current is mapped to the leak current (Fig. 6.15B). The axial resistance R_a is then identified to the membrane resistance and V_s to the leak reversal potential E_L. We may call this formal analogy a *model isomorphism*: variables of the resistive coupling model are mapped to those of an isopotential model, in a way that the electrical circuit is unchanged.

However, this is not the most convenient model isopmorphism, because in the resistive coupling model, the varied parameter V_s corresponds to E_L in the equivalent isopotential model, while all results where obtained by varying an injected current I. Instead, we can map the resistive coupling model to an isopential model with an injected current and a constant leak reversal potential (say equal to 0 mV) by identifying the axial current with the leak and injected current:

$$\frac{V_s - V_a}{R_a} = -\frac{V}{R} + I$$

This identity holds if we choose $V = V_a$, $R = R_a$ and $I = V_s/R_a$ (Fig. 6.15C). Thus, the resistive coupling model is equivalent to an isopotential neuron model with $E_L = 0$ mV and other variables as summarized below:

Isopotential model	Resistive coupling model
membrane potential V	axonal voltage V_a
membrane resistance R	axial resistance R_a
injected current I	V_s/R_a

6.2.3 Sharp spike initiation

Resistive coupling theory additionally postulates that the resistive coupling is strong enough that spike initiation becomes sharp (Brette, 2013), a phenomenon

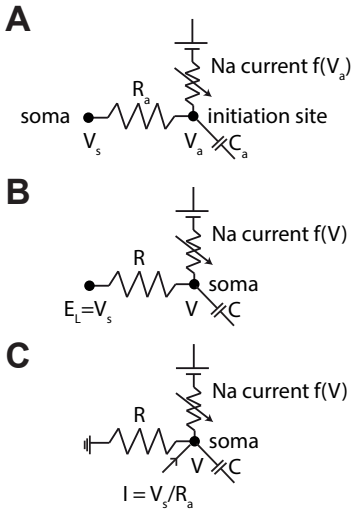

Figure 6.15: The resistive coupling model (A) is electrically equivalent to an isopotential models (B) and (C).

we will explain in this section. Briefly, sharp spike initiation refers to the phenomenon that axonal Na^+ channels open discontinuously as a function of somatic voltage, that is, there is a critical somatic voltage above which most axonal Na^+ channels suddenly open. This is phenomenologically similar to the cooperativity phenomenon (section 6.1.5), except that it relies on resistive coupling rather than inter-channel coupling.

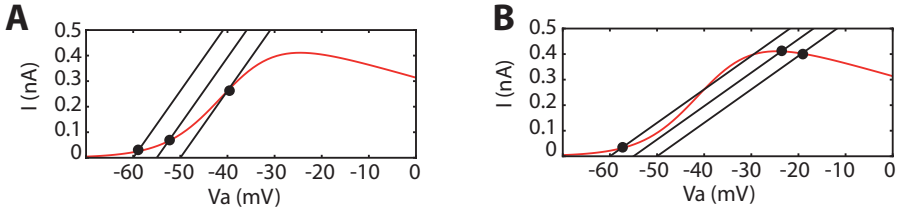

Figure 6.16: Bifurcation in the resistive coupling model (adapted from Brette (2013)). Sodium current (red) and axial resistive current (black) as a function of voltage at the initiation site when Na^+ channels are placed at 20 μm (A) and at 40 μm (B) away from the soma. The latter corresponds to a larger value of the coupling resistance R_a. The three lines correspond to somatic voltages of -60 mV, -55 mV and -50 mV.

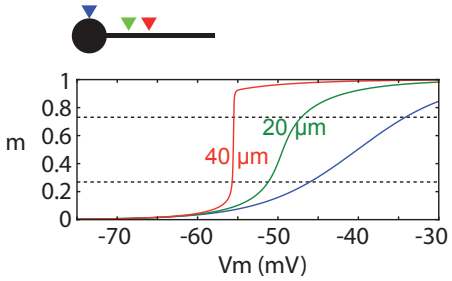

Figure 6.17: Proportion of open Na^+channels vs. somatic potential in a simple ball-and-stick model (adapted from Brette (2015)), where Na^+channels are placed at the location indicated by the arrow (only the location is varied).

Bifurcation in the resistive coupling model

In the resistive coupling model (Fig. 6.10), the resistive current equals the Na^+current, which means:

Relate to the equivalent isopotential model?

$$\frac{V_a - V_s}{R_a} = f(V_a)$$

where $f(V_a)$ is the Na^+ current as a function of axonal voltage. For a given value of the somatic voltage V_s, the value of V_a is determined by this fixed point equation. Figure 6.16 represents the two sides of this equation: the resistive current is an affine function of V_a, which equals 0 when $V_a = V_s$; the Na^+ current is a nonlinear function of V_a. The current and V_a are determined by the intersection of the two curves. We see in Fig. 6.16A that as V_s is increased, the axonal potential V_a gradually increases. However in Fig. 6.16B, where we have chosen a larger value for R_a, there is a value of V_s at which the resistive line is tangent to the Na^+ curve, and increasing V_s above that value makes the intersection point suddenly jump towards a higher value. Thus, V_a is a discontinuous function of V_s. We recognize in this phenomenon a bifurcation: as V_s is increased, the number of solutions to the fixed point equation changes from 1 to 3 to 1.

Concretely, this bifurcation means that axonal Na^+ channels open abruptly when the somatic voltage exceeds a threshold[6]. This is shown in Fig. 6.17, where the proportion of open Na^+ channels is plotted as a function of somatic voltage, for a model where channels are on the soma (blue), another where channels are on the axon but there is no bifurcation (green), and another where channels are further down the axon and there is a bifurcation (red). Seen from the soma, this is similar to increasing coupling in the cooperative model (section 6.1.5), except interchannel coupling is replaced by resistive coupling.

Signatures of sharp initiation

In voltage-clamp, sharp spike initiation means that all-or-none current spikes are measured at the soma when the holding potential is increased. This is

[6]Of course this opening is not instantaneous in reality. The speed of opening is limited by the axonal capacitance and activation time constant. These two factors are not included in the resistive coupling model.

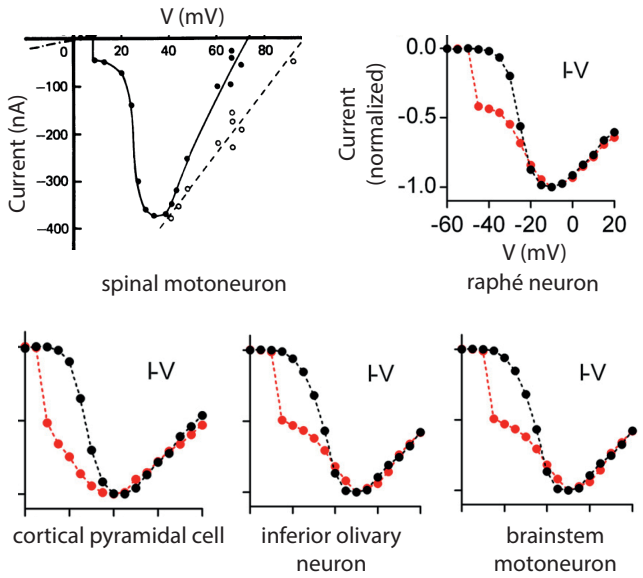

Figure 6.18: Relation between the peak Na^+current and voltage measured at the soma of various neurons. The first measurement was done with a two-electrode voltage clamp (Barrett and Crill, 1980) (voltage is relative to rest). Note the very large current at spike initiation (up to 400 nA). The other ones where done in patch clamp with the current reduced by TTX application and the contribution of somatic Na^+ channels has been subtracted (current is normalized to 1) (Milescu et al., 2010).

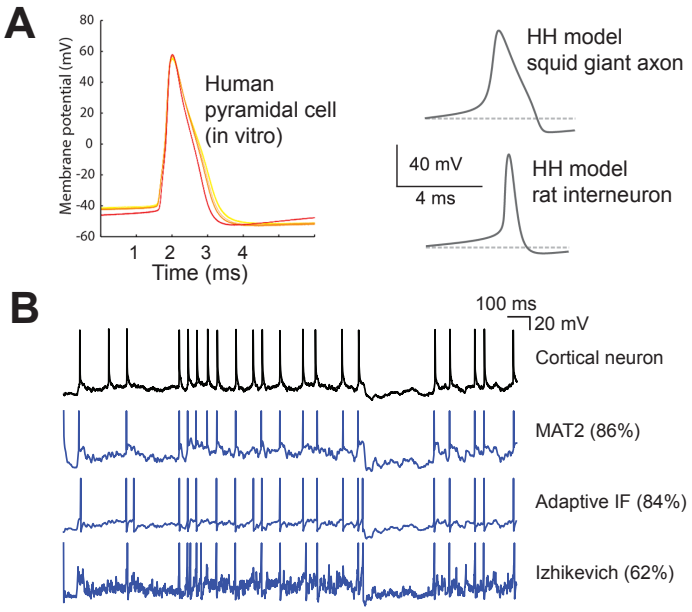

Figure 6.19: Signatures of sharp spike initiation. A, Action potential measured in a human pyramidal cell (Testa-Silva et al., 2014) and in two isopotential Hodgkin-Huxley models (Sengupta et al., 2010). B, Response of a cortical neuron in vitro to somatic current injection (black) and predictions by integrate-and-fire models with sharp spike initiation (blue, first two traces; percentages are proportion of correctly predicted spikes) and with smooth spike initiation (blue, third trace; the Izhikevich model, a variation of the quadratic model) (Rossant et al., 2011).

shown in Fig. 6.18, where the peak Na^+current is plotted as a function of holding voltage: we observe a discontinuous function. This phenomenon has been observed in many neurons[7], including motoneurons (Barrett and Crill, 1980), cortical, brainstem and raphé neurons (Milescu et al., 2010).

The current-voltage relationship can also be measured in somatic current-clamp, in neurons driven by noisy currents (Badel et al., 2008; Harrison et al., 2015). In cortical neurons, it was found that this relationship can be fitted by the sum of a linear function (representing the leak current) and an exponential function (representing the Na^+ current). Isopotential HH models, constrained by patch-clamp measurements of channel properties, predict that the curvature of the exponential function equals the Boltzmann activation slope $k_a = 6$ mV. Instead, the measured curvature is exceptionally sharp, on the order of 1 mV.

Sharp initiation also appears in the initial shape of spikes at the soma (Naundorf et al., 2006; Telenczuk et al., 2017). In isopotential Hodgkin-Huxley models, the onset of spikes is shallow because Na^+ channels open gradually with voltage:

[7]Such discontinuities can be produced in principle by incomplete compensation of the electrode resistance (which plays a similar role to the axonal resistance R_a) when the measured current is large, but this is not the case in these examples. Barrett and Crill (1980) used a two-electrode voltage-clamp, while Milescu et al. (2010) applied TTX to reduce the current so as to ensure proper voltage control.

membrane potential must increase by about 12 mV for the proportion of channels to rise from 27% to 73% (twice the Boltzmann activation slope k_a, which is about 6 mV). In contrast, there is a distinct kink at spike onset, which appears in a voltage trace as a rapid voltage transition from the resting membrane potential (Fig. 6.19A). This observation was the motivation for the cooperative model (see section 6.1.5), but is equally explained by resistive coupling theory. Below, we will present more precise predictions about the somatic spike onset.

In more detail, the presence of a saddle-node bifurcation also manifests itself in the dynamics of the potential near spike initiation. Indeed, as the bifurcation point is approached, the response to perturbations should slow down while the variance should increase[8]. Both phenomena are observed in cortical neurons, including in fast-spiking neurons, which have type II excitability (discontinuous current-frequency relation) (Meisel et al., 2015).

Finally, sharp spike initiation is also seen in the input-output properties of neurons (Brette, 2015). First, precise spiking responses of cortical neurons to noisy currents injected at the soma are surprisingly well predicted by integrate-and-fire models, which have a sharp threshold, unlike isopotential Hodgkin-Huxley models (Gerstner and Naud, 2009; Rossant et al., 2010, 2011) (Fig. 6.19B). Models with a smoother threshold (for example the quadratic model or the exponential model with a large slope factor) do not perform as well. Second, cortical neurons can reliably transmit frequencies up to several hundred Hz and respond to input changes at the millisecond timescale (Ilin et al., 2013; Tchumatchenko et al., 2011). This means that when a small high frequency sinusoidal current or a small current step is added on top of a background noisy current injected in the cell, the time-varying probability of discharge closely follows the input current. Again, this property is seen in integrate-and-fire models, but not in isopotential Hodgkin-Huxley models (Brunel et al., 2001; Fourcaud-Trocme et al., 2003).

Thus, phenomenologically, sharp initiation means that the response of a neuron to a somatically injected current is better modeled by an integrate-and-fire model, which has a sharply defined threshold on the somatic membrane potential, than by an isopotential Hodgkin-Huxley model. This may seem surprising as the Hodgkin-Huxley model is a more complex biophysical model that explicitly relates to biophysics of ionic channels. However, more complex does not mean more realistic (see Brette (2015) for a discussion of this epistemological point).

Conditions for sharp initiation

Sharp initiation does not occur as soon as spikes initiate in the axon. This can be seen in Fig. 6.16, which explains the bifurcation in the resistive coupling model: the bifurcation occurs only if the Na^+ current increases more steeply with axonal voltage than the resistive axial current. Thus, there needs to be a sufficiently strong Na^+ conductance, or the channels must be placed far enough from the soma. In fact, this is analog to the excitability condition of an isopotential model (see chapter **??**): the model is excitable if the Na^+ current increases more steeply with membrane potential than the resistive leak current. The bifurcation point in the resistive coupling model corresponds to the spike threshold for slow inputs

[8] This is because this bifurcation corresponds to a stable point that becomes unstable.

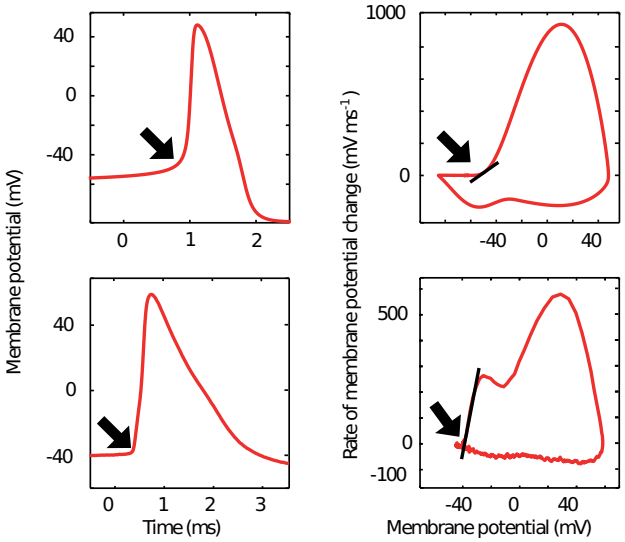

Figure 6.20: Onset rapidness in an isopotential model (top) and in a human pyramidal neuron (bottom, from Testa-Silva et al. (2014)). Left: action potential; right: phase plot (dV/dt vs. V). The arrow shows the spike onset (determined as the point where $dV/dt = 20$ mV/ms) and the black line is a regression line whose slope is onset rapidness: 5.6 ms^{-1} in the isopotential model, 28.8 ms^{-1} in the human neuron. Adapted from Telenczuk et al. (2017).

(I is a constant parameter) in the equivalent isopotential model. We have seen in chapter **??** that for this bifurcation to occur, the ratio of Na^+ conductance to leak conductance (denoted p) must be large enough. With the Boltzmann model of channels, this condition is:

This is actually in old version of chapter 4, 4.4.5

$$p > \frac{k_a}{E_{Na} - V_{1/2} - 2k_a}$$

where k_a is the activation Boltzmann slope factor of the Na^+ channels and $V_{1/2}$ is their half-activation voltage[9]. For the resistive coupling model, this ratio corresponds to the ratio of Na^+ conductance to axial resistance: $p = g_{Na}.R_a$. To give an order of magnitude, with $E_{Na} = 60$ mV, $V_{1/2} = -40$ mV, $k_a = 6$ mV, the condition is

$$g_{Na}.R_a > 0.27$$

Thus, for a given Na^+ conductance, spike initiation becomes sharp when the initiation site exceeds a critical distance from the soma.

Somatic onset rapidness

Experimentally, the sharpness of spike initiation has been assessed from the shape of the somatic action potential, using a measure called *phase slope* (Naundorf et al., 2006). Phase slope is the slope of the curve representing dV/dt

Possibly reorganize: define onset rapidness as max phase slope

[9]The formula can be amended for the GHK model.

as a function of V; it has dimensions of second^{-1}. In the time domain, it is determined by the following formula:

$$\eta = \left(\frac{d^2V}{dt^2}\right) / \left(\frac{dV}{dt}\right)$$

Onset rapidness is the phase slope at spike onset. Thus, it depends on the criterion for spike onset, typically a condition on dV/dt. However, when measured on the somatic action potential of many neurons, onset rapidness varies only weakly with this criterion, and is typically about 20 ms^{-1} (Baranauskas et al., 2010) (Fig. 6.20). Note that in experimental conditions, this is a very imprecise measurement.

We will now examine the prediction of resistive coupling theory. First, let us start with an isopotential model (see Fig. 6.20A). If we write $dV/dt = f(V)$, then phase slope is $\eta = f'(V)$. Let us consider the spike initiation zone where the Na^+ current is the main current. This current depends on V in an approximately exponential way, $I \propto e^{-V/k}$, where k is the Boltzmann activation factor (about 6 mV). Therefore, $\eta = f'(V) \approx f(V)/k$. Thus, in an isopotential model, onset rapidness is:

$$\eta = \frac{1}{k}.\frac{dV}{dt}$$

With $dV/dt = 20$ mV/ms, the isopotential model should have an onset rapidness of roughly[10] 3–4 ms^{-1}. We note that onset rapidness is critically dependent on the spike onset criterion, contrary to the findings on somatic action potentials.

Before we turn to the somatic spike, let us consider the AIS spike. We assume, following the assumptions of resistive coupling theory, that the somatic voltage does not vary significantly in the time of interest, and the AIS is coupled resistively to the soma. Since we are interested in the dynamics, let us consider now the local capacitance of the AIS (and proximal axon). We can see that we obtain a model that is identical to an isopotential model, except that the leak current is replaced by the axial resistive current towards the soma. It follows that the phase slope has the same properties as in an isopotential model. Empirically, onset rapidness can be measured in the AIS, although it is technically difficult because of its small size. For example, Yu et al. (2008) measured a value of 5.6 ms^{-1} in an axonal bleb (with $dV/dt = 20$ mV/ms), a little above the predicted value.

Let us now examine the phase slope of the somatic action potential. At spike initiation, the soma receives a strong axial current from the initial segment. Thus, the membrane equation is approximately:

$$C\frac{dV}{dt} = I$$

where I is the axial current. Phase slope is therefore:

$$\eta = \frac{dI}{dt}/I$$

According to the resistive coupling hypothesis, the axial current is:

$$I = \frac{V_a - V}{R_a}$$

[10] As we have neglected outward currents, this is an underestimation.

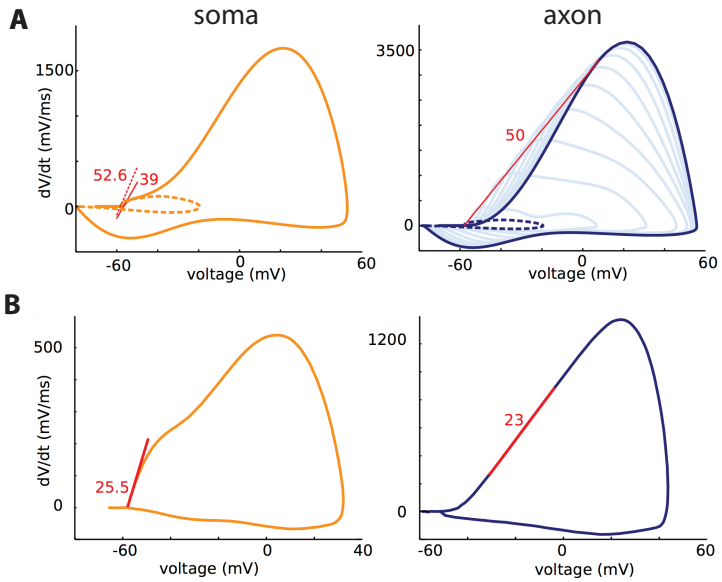

Figure 6.21: Relation between somatic onset rapidness (left) and dynamics of the axonal spike (right), adapted from Telenczuk et al. (2017). A, Left: somatic onset rapidness defined as maximum phase slope in a detailed biophysical model, with (solid) and without (dashed) somatic Na^+channels (somatic Na^+channels perturbs the measurement). Right: Spike at different positions along the AIS (the largest at the distal end), with the tangent line passing through threshold in red, whose slope is theoretically equal to somatic onset rapidness. B, Spike in a pyramidal cortical neuron recorded at the soma (left)and axon (right), showing a similar maximum phase slope (adapted from Yu et al. (2008)).

where V_a is the voltage at the AIS, and V is the somatic voltage that we assume approximately constant. In other words, V is the somatic voltage threshold. Therefore, phase slope is

$$\eta = \frac{dV_a}{dt}/(V_a - V)$$

Graphically, in the axonal phase plot (dV_a/dt vs. V_a), this is the slope of a line that goes from spike onset to a point on the phase plot (Fig. fig-onset-rapidness-calculationA). As mentioned above, experimental measurements report a roughly constant value of somatic onset rapidness, as a function of spike onset criterion. This means that the somatic phase slope is measured near its (local) maximum. In the axonal phase plot, the maximum of $(dV_a/dt)/(V_a - V)$ is the slope of a tangent to the spike going through threshold. This is approximately equal to the maximum value of dV_a/dt divided by axonal spike height, $V_a - V \approx 100$ mV, or to the maximum axonal phase slope (a slight overestimate).

In other words, resistive coupling theory predicts that somatic onset rapidness directly reflects the speed of the axonal spike. For example, in recordings of a cortical pyramidal neuron (Yu et al., 2008), maximum phase slope is 23 ms^{-1} in the axonal bleb near the AIS and 25.5 ms^{-1} in the soma (Telenczuk et al., 2017) (Fig. 6.21B).

6.2.4 The spike threshold

Axonal spike threshold

In the resistive coupling model, under the conditions derived above, the Na^+ channels open abruptly when the somatic membrane potential V_s exceeds a certain value. Thus, there is a bifurcation with respect to V_s. In the equivalent isopotential model, this corresponds to a bifurcation with respect to the current I. We have seen that with the Boltzmann model, the bifurcation occurs when:

$$V \approx V_{1/2} - k \log \left(\frac{g_{Na}}{g_L} \frac{E_{Na} - V_{1/2}}{k} - 1 \right)$$

The term -1 is a small correction which may be omitted for simplicity (it then corresponds to the formula for the exponential model). If we translate this threshold equation back into the coupling resistive model, we obtain:

$$V_a \approx V_{1/2} - k \log \left(g_{Na} R_a \frac{E_{Na} - V_{1/2}}{k} - 1 \right)$$

This is the axonal spike threshold (first derived in Brette (2013)). The somatic spike threshold corresponds to the rheobase in the isopotential model. We will derive it by calculating the axial current at threshold.

Sodium current at threshold

The axial current equals the sodium current $f(V_a) = g_{Na} m(V_a)(E_{Na} - V_a)$, where m is the activation function. Threshold is defined by the bifurcation equation:

$$\frac{1}{R_a} = f'(V_a)$$

If we use the exponential model of excitability[11], then we have $f' = f/k$, where k is the activation slope factor. It follows that the sodium current at threshold is

$$f(V_a) = \frac{k}{R_a}$$

Somatic spike threshold

Since the sodium current equals the axial resistive current, which follows an ohmic relation, the voltage gradient between soma and axonal initiation site is just:

$$V_a - V_s = k$$

From this, we deduce that the somatic spike threshold is $V_a - k$, that is:

$$V_s \approx V_{1/2} - k - k \log \left(g_{Na} R_a \frac{E_{Na} - V_{1/2}}{k} - 1 \right)$$

[11] which is accurate far below half-activation voltage.

Which spike threshold matters for excitability?

It may seem disconcerting that there are several spike thresholds. Which one is relevant for excitability, the somatic or the axonal one? At first sight, it might seem that it is the axonal threshold that matters, since the initiation site is in the axon. This is a mistake. Indeed, the bifurcation parameter that determines whether the neuron spikes is the somatic voltage V_s. It plays the same role as the current I in the equivalent isopotential model. This appears more clearly when we ask what is the threshold input that makes the neuron spike, whether current or charge. Since the somatic voltage is the bifurcation parameter, it determines both the current and charge thresholds, as follows:

This might be more meaningful after we discuss modulation by AIS currents

$$\begin{aligned} \text{Current threshold:} \quad & (V_s - E_L)/R_m \\ \text{Charge threshold:} \quad & (V_s - E_L)/C_m \end{aligned}$$

where V_s is the somatic spike threshold, R_m is the input resistance at the soma, and C_m is input capacitance at the soma.

Of course, in our formulas, axonal and somatic thresholds are directly related, and only differ by a constant term k. However, we will see later that AIS currents can modulate the somatic spike threshold with little impact on the axonal spike threshold, and it is the former that determines excitability.

Maximum threshold

We have seen that sharp initiation only occurs if $g_{Na}R_a$ is large enough. When $g_{Na}R_a$ is reduced, the threshold increases, until sharp initiation (i.e., the bifurcation) disappears. What is the highest possible value for the threshold? This is the value obtained at the critical point where the bifurcation disappears. This is in fact the same formal problem as the condition for excitability derived for the isopotential model in section **??**, where E_L is mapped to V_s (derived in appendix **??**). For the resistive coupling model, this condition is: $V_{1/2} = V_s + 2k$. Thus, the somatic spike threshold cannot be higher than $V_{1/2} - 2k$. For example, with $V_{1/2} = -30$ mV and $k = 6$ mV, we obtain a maximum spike threshold of -42 mV.

6.2.5 The spatial extent of the AIS

Until now, we have considered a simplified resistive model where all Na^+ channels are clustered in a single point on the axon. We now examine a spatially extended AIS in the context of resistive coupling theory.

Initiation site vs. site of sodium entry

When considering the spatial extent of the AIS, resistive coupling theory implies that the electrical initiation site, the point where the potential first increases, does not necessarily match the point where Na^+ first enters the axon. This counter-intuitive implication stems from the fact that the soma clamps the beginning of the axon. If we neglect all passive transmembrane currents (capacitive and resistive), then according to cable theory:

$$\frac{\partial^2 V}{\partial x^2} \propto -I_{Na}(x)$$

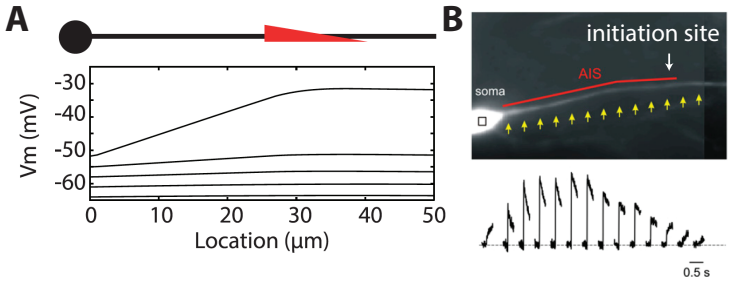

Figure 6.22: Initiation site vs. site of sodium entry. A, Voltage vs. distance from the soma in a simple ball-and-stick model with non-inactivating Na^+channels, at different values of somatic V_m (Brette, 2013). Here the AIS has more Na^+channels on the proximal side but the $V_m(x)$ is still an increasing function of x. B, Fluorescence measurement of Na^+influx at spike initation in the AIS of a cortical pyramidal neuron (Baranauskas et al., 2013). Maximum influx is in the proximal part of the AIS even though spikes initiate at the distal end.

This implies that the spatial voltage profile is an increasing and concave function of distance (Fig. 6.22A), and most significantly: 1) spike initiation always occurs at the end of the AIS (in the sense of a criterion on V); 2) the maximum flow of Na^+ current occurs not at the distal end but somewhere between the soma and the AIS[12]. This is exactly what was found with Na^+ imaging of the AIS (Baranauskas et al., 2013), as shown on Fig. 6.22B.

Note that the influx of Na^+into the AIS does not directly reflect the density of Na^+channels. In fact, the maximum influx of Na^+would still occur on the proximal side even if Na^+channels were evenly distributed along the AIS. This is because the Na^+current density is $I_{Na} = g_{Na}(E_{Na} - V)$, and the driving force is larger on the proximal side because the soma clamps the proximal side of the axon (see e.g. simulated axonal spikes on Fig 6.21A).

The spike threshold with an extended AIS

Research in progress.

6.2.6 AIS geometry and excitability: experimental observations

First, we note that the formula for the spike threshold is virtually the same as in the isopotential case, except the leak conductance is replaced by the inverse axial resistance. Therefore, all the remarks made in section **??** apply. The new aspect that appears in our revised formula is the dependence on axial resistance R_a. That resistance depends on the geometry of the AIS. In this simplified model where all channels are clustered at one point in the axon, this resistance is proportional to the distance between the soma and the initiation site (assuming constant axon diameter). Thus, spike threshold decreases (the neuron becomes more excitable) when the initiation site is moved distally from the soma. This

[12]Precisely, where $\partial^3 V/\partial x^3 = 0$

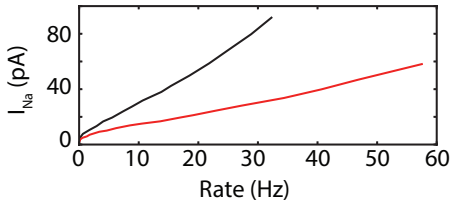

Figure 6.23: Energy consumption for axonal vs somatic initiation (adapted from Brette (2013)). A ball-and-stick model is stimulated with fluctuating current at the soma, and the average Na^+current is shown as a function of firing rate for axonal (red) and somatic (black) spike initiation.

counter-intuitive result can be explained by the fact that the initiation site is then more electrically isolated from the large soma.

TODO.

6.2.7 Energetic considerations

This could be in a separate chapter about energy

Is it more energetically efficient to initiate spikes in the axon rather than in the soma? The benefit of axonal initiation is obvious if there is no somatic action potential, since then no energy is spent on charging the somatic capacitance. Otherwise, in either case, the entire membrane of the neuron needs to be charged, which implies moving a positive charge equal to $C\Delta V$, where C is the total capacitance of the neuronal membrane and $\Delta V \approx 100$ mV is the spike height (assuming no overlap with outward currents). Thus, the cost of generating of a spike does not depend very much on the site of spike initiation.

However, there is a difference in the energetic consumption below threshold, which leads to more energetically efficient spike initiation with a distal initiation site. This is illustrated in Fig. 6.23, which shows the average Na^+ current as a function of firing rate, in a ball-and-stick model (soma plus short unmyelinated axon) stimulated by a fluctuating current. For the same firing frequency, a smaller Na^+ current is produced when spikes are initiated in the AIS than in the soma.

As we have seen previously, the sodium current at threshold is k/R_a. Thus, there is less current at threshold when the spike initiation site is more distal. This reflects the fact that the axonal initiation site is easier to excite when it is more isolated from the soma. At a given distance ΔV below threshold, the current would be about

$$I_p = \frac{k}{R_a} e^{-\Delta V/k}$$

This is called the *persistent Na^+ current* (Astman et al., 2006), and it determines the energetic cost of excitability, independently of whether the neuron produces spikes. Remarkably, for a given voltage threshold, this current does not depend on either conductance density or half-activation voltage. For an axon of fixed diameter, it is inversely proportional to the distance of the initiation site from the soma. With $k = 6$ mV and $R_a = 40$ MΩ, we obtain a threshold current of $I_p = 150$ pA. At a distance $2k$ below threshold, the current is about $I_p \approx 20$ pA.

How does this compare with the cost of producing a spike? This cost is proportional to the total membrane area of the neuron. In the grey matter of rodent brains (i.e., unmyelinated neurons), the total Na^+ charge required to produce a spike was estimated at 184 pC (Attwell and Laughlin, 2001), based on 4 cm of axon of diameter 0.3 μm. This estimate is based on the assumption that the Na^+ charge necessary to produce an action potential is 4 times the minimal value given by the membrane capacitance (because of overlap with the K^+ current), but recent estimates of this efficiency factor point to a value of about 2 in cortical pyramidal cells (Hallermann et al., 2012). Thus, each spike should require moving a Na^+ charge of around 90 pC. The average Na^+ current necessary to produce spikes at frequency F is therefore:

$$I_{\text{spike}} = 90 \text{ pC}.F$$

Thus, at frequency $F = 1$ Hz, this current is about 90 pA. This is a similar magnitude as the persistent current I_p necessary for excitability. The balance between the cost of spikes and the cost of excitability depends on firing frequency and neuron size.

6.3 Resistive coupling theory: spike transmission to the soma

In cortical pyramidal neurons, as well as in many other neurons, the action potential is initiated in the AIS, and then it backpropagates to the soma and dendrites. This signal can be important for synaptic plasticity. There are also voltage-gated calcium channels at the soma that are involved in the regulation of metabolic processes, and therefore it may be functionally important that action potentials are transmitted to the soma. This requires the axonal spike to produce a sufficient depolarization of the soma, so that somatic Na^+channels are recruited and regenerate the action potential. Thus we ask the question: what determines the amount of current transmitted to the soma by an action potential initiated at the AIS?

6.3.1 The axonal current transmitted to the soma

An incorrect intuition

How much current is transmitted to the soma at spike initiation? Since this current originates from the transmembrane Na^+ current at the AIS, and that current is proportional to the total Na^+ conductance g_{Na}, it may seem at first sight that the current transmitted at spike initiation is proportional to g_{Na}. This is incorrect. The flaw in the reasoning is that the Na^+ current is also proportional to the driving force $E_{Na} - V_a$, and that driving force approaches 0 during the axonal action potential. We first show that an essential determinant of the transmitted current is the geometry of the system, then we look in more detail at the role of Na^+ conductance.

A first approximation

In the resistive part of the axon, between the soma and the edge of the AIS, the axial current is determined by Ohm's law: $I_a = (V_a - V_s)/R_a$, where R_a is the

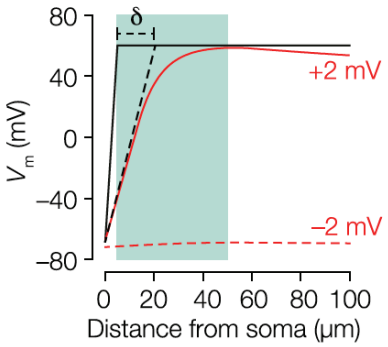

Figure 6.24: Voltage along the axon at spike initiation in a simple cylindrical model clamped at the proximal end (Hamada et al., 2016), with the AIS represented in green. The solid black line shows the (idealized) voltage profile when Na^+channels clamp the axon at E_{Na}. The solid red curve shows the voltage when Na^+channels are all open but in finite number, with somatic potential just above threshold (dashed: just below threshold). The transmitted current is equivalent to the idealized case with an AIS starting at an extra distance δ.

axial resistance between the soma and the start of the AIS. At spike initiation, the membrane potential at the AIS increases very quickly towards its peak, and in that duration the somatic potential increases only modestly above threshold (see Fig. 6.7). Thus, in calculating the axial current at spike initiation, we can consider that the somatic membrane potential is near threshold while the membrane potential in the AIS is near its peak.

Let us start with a drastic approximation: we consider that the AIS is clamped at the Na^+ reversal potential, $V_a = E_{Na}$, while the soma is at threshold V_s. Between the soma and the start of the AIS, the voltage increases linearly (assuming cylindrical geometry), then is constant, as shown on Fig. 6.24 (solid black curve). This corresponds to the approximation of infinite Na^+ conductance density in the AIS, with a large soma. The axial current is then $I_a = \Delta V/R_a$, where $\Delta V = E_{Na} - V_s \approx 100$ mV. We find that the axial current is essentially determined by the axial coupling resistance between soma and AIS, and therefore by the geometry of the spike initiation system. For an axon of constant diameter, the axial current is inversely proportional to the distance of the start of the AIS from the soma.

This effect can be seen in biophysical models of spike initiation (Telenczuk et al., 2017). In Fig. 6.25, an excitable model consisting of two cylinders, one from the soma and one for the axon, is simulated. There are Na^+ and K^+ channels in the soma and in the AIS, which is represented as a single point (all channels clustered at the same position). The effect of varying the position of the AIS is seen most clearly in the first of component of the phase plot. When the AIS is more proximal, spikes are initiated at a higher voltage but produce a smaller axial current (small dV/dt). Thus, there is an inverse relation between excitability and transmission to the soma. This is most clearly seen when plotting the maximal amplitude of the axial current recording in a somatic voltage clamp, as a function of clamping voltage (starting from rest) (Fig. 6.25B). There

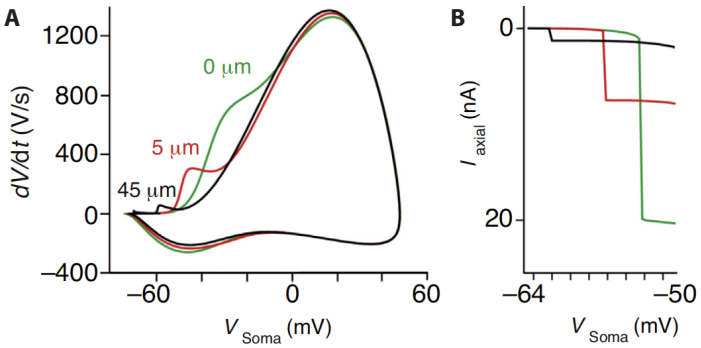

Figure 6.25: Effect of AIS position on the current transmitted to the soma (adapted from (Telenczuk et al., 2017)). A two-cylinder biophysical model representing soma and axon are simulated, with Na^+channels clustered at one point on the axon. A, Phase plot of the action potential for three different distances of the AIS. B, Peak current transmitted to the soma vs. somatic potential in voltage-clamp.

is a threshold above which the axonal spike is triggered, so that the current-voltage relation is discontinuous. We can see clearly that there is an inverse relation between the somatic voltage threshold and the axial current.

The effect of Na^+ conductance

Quantitatively, our formula is an approximation that is only valid in the limit of an infinitely large Na^+ conductance, so that $V_a = E_{Na}$. Let us see what happens when we consider a finite conductance g_{Na} positioned at a single point in the axon. We assume that at the peak of the axonal action potential, the membrane potential is well above half-activation voltage so that all available Na^+ channels are open. Then the Na^+ current is $I_{Na} = g_{Na}(E_{Na} - V_a)$. Matching this current with the axial resistive current gives:

$$g_{Na}(E_{Na} - V_a) = \frac{V_a - V_s}{R_a}$$

Thus, the peak axonal voltage is

$$V_a = E_{Na} - \frac{1}{1 + R_a g_{Na}}(E_{Na} - V_s)$$

The axial current is then:

$$\begin{aligned} I_a &= \frac{g_{Na}}{1 + R_a g_{Na}}(E_{Na} - V_s) \\ &= \frac{E_{Na} - V_s}{R_a}\left(1 - \frac{1}{1 + R_a g_{Na}}\right) \end{aligned}$$

Thus, Na^+ conductance has an effect on the axial current, but that effect is not linear: it saturates at $(E_{Na} - V_s)/R_a$.

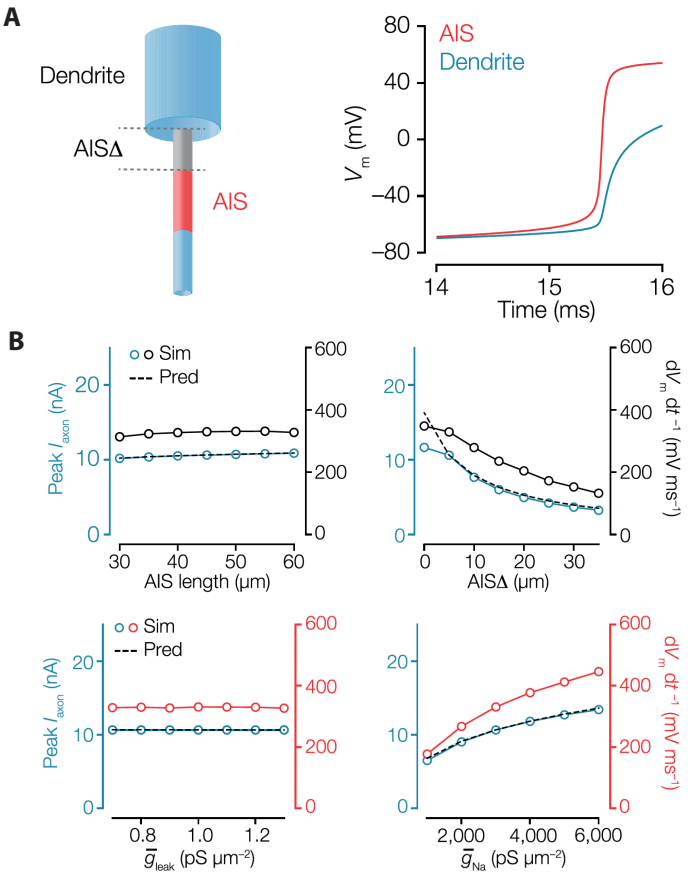

Figure 6.26: Current transmitted to the soma as a function of biophysical parameters (adapted from Hamada et al. (2016)). A, A two-cylinder model representing soma and axon are simulated, with non-inactivating Na^+channels distributed along the AIS (and no other channel). The model is simulated in either somatic current-clamp (right) or voltage-clamp (blue in B-E). B, Peak axial current (blue) and predicted value (dashed) in voltage-clamp and maximum somatic depolarization in current-clamp (black and red), as a function of different biophysical parameters.

The spatial extent of the AIS

We now consider the more realistic case when Na^+ channels are spatially distributed on a cylindrical AIS of length L and diameter d, starting at distance $x = \Delta$ from the soma, as shown on Fig. 6.26A. Let g be the surfacic Na^+ conductance density, so that the total conductance is

$$g_{Na} = \pi d L g$$

The AIS is connected to the soma through an axial resistance $R_a = r_a x$, where

$$r_a = \frac{4R_i}{\pi d^2}$$

is the axial resistance per unit length of axon. As before, we only consider the axial resistive current and the Na^+ current, assuming that all channels are open. Matching these two currents in the AIS (between $x = \Delta$ and $x = \Delta + L$) gives the following simplified cable equation:

$$\frac{1}{r_a} V'' = -\pi d g (E_{Na} - V)$$

where $V(x)$ is the membrane potential at distance x from the soma. In the resistive part of the axon (between $x = 0$ and $x = \Delta$), the equation is just $r_a V'' = 0$, which means that $V(x)$ is a linear function of x. Thus we have a second order differential equation, and two boundary conditions: 1) the potential at the soma is $V(0) = V_s$, and 2) no axial current flows at the end of the AIS towards the axon: $V'(\Delta + L) = 0$.

Since voltage is linear in the resistive part of the axon, the first boundary condition can be replaced by:

$$V(\Delta) = V_s + V'(\Delta)\Delta$$

We then solve this second order equation (sum of two exponential functions), and we obtain the voltage profile $V(x)$ along the axon, as shown in Fig. 6.24 (red curve). The axonal current flowing into the soma is given by the initial slope of this profile, specifically:

$$I_a = \frac{V'(0)}{r_a} = \frac{V'(\Delta)}{r_a}$$

We obtain the following expression:

$$I_a = \frac{E_{Na} - V_s}{r_a(\Delta + \delta)}$$

where

$$\delta = \frac{\sqrt{\frac{d}{gR_i}}}{2 \tanh \sqrt{\frac{4R_i g}{d}} L}$$

For large AIS length and conductance density (typical values), this is close to:

$$\delta \approx \frac{1}{2}\sqrt{\frac{d}{gR_i}}$$

which has dimensions of length. Remarkably, this makes the axial current independent of AIS length. A physical interpretation of this formula is that an extended AIS with finite conductance density produces a current that is equivalent to that of an AIS with infinite conductance density (which clamps the potential at E_{Na}) positioned further away from the soma, by a distance δ (dashed black line in Fig. 6.24).

This analytical calculation is matches quite accurately the peak current measured in voltage-clamp simulations of a cylindrical axon with non-inactivating Na^+channels (and no other channels), as shown on Fig. 6.26B. For very proximal AIS (small Δ), the calculation is an overestimation of the actual current. This is because the proximal end of the AIS is then clamped near somatic potential, and therefore not all Na^+channels are open, as is assumed in the calculation. The plots also show the depolarization at the soma in current clamp, when a large cylindrical process is attached, representing soma and dendrite. The variations of this depolarization with the different parameters follows quite well (but not exactly) those of the axial current measured in voltage-clamp.

Tapering of the axon hillock

We have assumed that the axon is cylindrical. However, there is typically tapering at the start of the axon before it becomes approximately cylindrical. If tapering occurs within the AIS, there is no simple way to integrate it analytically in the theoretical predictions. But if tapering occurs before the AIS, then it is easy to incorporate it, by calculating the total axial resistance between the soma and the start of the AIS by integration:

$$R_a = \frac{4R_i}{\pi}\int_0^{\Delta}\frac{1}{d(x)^2}dx$$

where $d(x)$ is the axon diameter at distance x from the soma and the axial current is then:

$$I_a = \frac{E_{Na} - V_s}{R_a + r_a\delta}$$

Minimum Na^+ conductance density

We can use this formula to calculate the minimum Na^+ conductance density necessary to produce a given axial current. Let us consider the case when the entire axon has a homogeneous conductance density g. This will produce an axial current greater than any AIS with the same density g. According to our calculations, the current will be:

$$\begin{aligned} I_a &= 2\frac{E_{Na} - V_s}{r_a\sqrt{\frac{d}{gR_i}}} \\ &= \frac{\pi}{2}\sqrt{\frac{g}{R_i}}d^{3/2}(E_{Na} - V_s) \end{aligned}$$

It follows that the minimum conductance density to produce an axial current I_a is:

$$g_{\min} = \frac{4R_i}{\pi^2 d^3}\Big(\frac{I_a}{E_{Na} - V_s}\Big)^2$$

To obtain a lower bound when there is tapering, we simply choose d as the largest axon diameter along the AIS.

Let us consider for example a layer 5 cortical pyramidal neuron of a rat. It has an input capacitance at the soma of about $C \approx 250$ pF (Arsiero et al., 2007), and dV/dt reaches a peak of about 250 mV/ms in the first phase of the somatic spike. This should correspond to an axial current of about $I_a = CdV/dt = 62.5$ nA. It is likely that this is overestimated, because the input capacitance estimate includes a large part of the dendrites, while on a short time scale dendrites would contribute less. In a biophysical model of layer 5 pyramidal cell which gives realistic values for dV/dt (Hallermann et al., 2012), the axial current is about $I_a = 25$ nA. Let us now choose $R_i = 150$ Ω.cm, $d = 1.5$ μm, $E_{Na} - V_s = 100$ mV. We find that the minimum conductance density is about $g_{\min} = 11250$ ps/μm^2. This is indeed much higher than the conductance density measured at the soma.

An interesting aspect of this formula is that it makes a prediction about how the diameter of the AIS should scale with the diameter of the soma. Let us consider a spherical soma and ignore the dendrites. The somatic capacitance scales as d_{soma}^2, and therefore so does the axial current necessary to charge it. It follows that, if the AIS conductance density is fixed (or at least, presumably, bounded), then our formula implies that d_{AIS}^3 should scale as d_{soma}^4, that is, $d_{\text{AIS}} \propto d_{\text{soma}}^{4/3}$. This is indeed consistent with measurements (Fig. 6.2).

6.3.2 Matching between soma and AIS geometry

The axial current transmitted at spike initiation to the soma determines the somatic depolarization. In turn, this depolarization opens somatic Na^+ channels, which regenerate the action potential at the soma, as shown on Fig. 6.1. Thus, the axial current must be strong enough that the threshold of somatic channels is reached. In addition, in terms of energy consumption, it is most efficient if this current is strong enough, but not stronger. Therefore, to efficiently transmit the axonal spike to the soma, the axial current must be tuned so as to depolarize the soma by the right amount.

If the Na^+ conductance density is fixed, this tuning requires adjusting the position and length (but mostly the position) of the AIS.

Matching AIS geometry to a spherical soma

Let us a start with an isopotential spherical soma of diameter d_{soma}. This soma has a membrane capacitance $C = \pi d_{\text{soma}}^2 c_m$, where c_m is the specific membrane capacitance. When we determined the conditions of excitability, we looked at one piece of the current loop shown in Fig. 6.6: Na^+ current matches the resistive axial current. To determine the depolarization due to the axial current, we look at the next piece of the current loop: resistive axial current matches the capacitive current, which means:

$$C\frac{dV}{dt} = I$$

where I is the axial current.

Thus, the amount of current necessary to depolarize the soma is proportional to the area of the soma. If the soma is larger, then we need a larger current

and therefore the AIS must be closer to the soma. In other words, we predict an inverse relation between soma size and AIS position.

With the simplest approximation, $I \propto 1/x$, where x is AIS position, everything else being equal. It follows that

$$x \propto d_{\text{soma}}^{-2}$$

With the more precise calculation, $I \propto 1/(x+\delta)$, where δ is a shift that depends on conductance density and AIS diameter (in fact, roughly on the space constant of the AIS). It follows that matching the axial current to the somatic capacitance requires the following scaling:

$$x = \alpha d_{\text{soma}}^{-2} - \delta$$

where α is a proportionality factor.

If we now examine the influence of AIS diameter in the simple approximation, we note that $I \propto 1/(r_a x)$, and since $r_a \propto d_{\text{AIS}}^{-1/2}$, we obtain:

$$x \propto d_{\text{soma}}^{-2} d_{\text{AIS}}^{1/2}$$

Thus, AIS position is negatively correlated with soma size, and positively correlated with axon diameter.

We have noted before that across neurons, soma and AIS diameters are correlated by a power law with exponent around 3/2 or 4/3 (see Fig. 6.5). It follows that, across neurons, AIS position should scale as $x \propto d_{\text{soma}}^{-4/3}$ or $x \propto d_{\text{soma}}^{-5/4}$. One might have thought that across neurons of different sizes, the entire subcellular structure would scale, with larger neurons having an AIS further away from the soma. Instead, we thus arrive at the counter-intuitive conclusion that the position of the AIS should be inversely related to the size of the neuron. The difficulty with testing this prediction is that many neurons have extended dendrites, which also contribute to the input capacitance at the soma. Thus, we now consider the impact of dendrites on this prediction.

Matching AIS geometry to a cylindrical somatodendritic process

We previously considered the soma as an isopotential compartment. In reality, when the soma receives the current spike from the axon, current also leaks towards the dendrites. In other words, the axial current charges not only the soma, but also part of the dendrites. How much of the dendrites should be considered? This depends on the time scale of the current: a constant current would charge a dendritic length of order λ, the space constant of the dendrite, but a transient current would charge a much smaller length of dendrite. We can get a rough order of magnitude by looking at the space constant $\lambda(f)$ for a time-varying current of frequency f (section **??**), which is at high frequency:

$$\lambda(f) \approx \frac{\lambda}{\sqrt{\pi f \tau}} = \sqrt{\frac{d}{4\pi R_i f c_m}}$$

Let us assume that the first phase of the somatic spike is about 0.1 ms; this would correspond to a frequency of roughly $f = 1/(0.2 \text{ ms})$. With $d = 6$ μm, $R_i = 120$ Ω.cm and $c_m = 0.9$ μF/cm^2, we obtain $\lambda(f) \approx 66$ μm. This

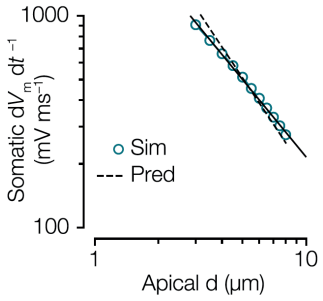

Figure 6.27: Maximum somatic depolarisation speed due to the axonal spike vs. dendrite diameter in the two-cylinder model of Fig. 6.26A (adapted from Hamada et al. (2016)). Dashed line: expected $d^{-3/2}$ scaling; solid line: linear regression.

is of course a crude estimate, but it indicates only the proximal dendrites are initially charged by the axial current at spike initiation. This corresponds to membrane area of about 1000 μm^2. As a comparison, the membrane area of a spherical soma of diameter 30 μm is about 2800 μm^2; thus, a similar order of magnitude.

An important point to notice is that the dendritic length to consider depends on the morphology of the dendrites (d) and intrinsic parameters that are in principle very similar across neurons (R_i and c_m), but it does not depend on resistive properties of the membrane, i.e., on channels (including leak channels).

We now examine a simple case that is analytically tractable: the soma and dendrites form a single cylinder of fixed diameter and large length (as in Fig. 6.26A). This is a rough model of the morphology of layer 5 pyramidal cells of the cortex, which have a large apical dendrite (roughly 6 μm). In this case, we know that the space constant for a given frequency is proportional to $\sqrt{d}$, and therefore the membrane area of a characteristic length of dendrite scales as $d^{3/2}$. Therefore, the current required to charge the soma and proximal dendrite scales as $d^{3/2}$.

A more precise analysis is to look at the impulse response of cylindrical dendrite (i.e., semi-infinite cylinder) to a current. This has been derived by Rall (1969):

$$G(t) = \frac{1}{C^*} \frac{e^{-t/\tau}}{\sqrt{\pi t/\tau}}$$

where C^* is the capacitance of a characteristic length of dendrite:

$$C^* = \pi d^{3/2} \sqrt{\frac{R_m}{R_i}} c_m$$

We recover the result obtained above from scaling considerations, i.e., the depolarisation for a given current scales as $d^{-3/2}$. Fig. 6.27 shows the somatic depolarization speed due to the axonal spike in the two-cylinder model of Fig. 6.26A, as a function of dendrite diameter (the soma is not excitable). Here the depolarisation scales as $d^{-1.22}$. The reason for the imperfect scaling is that we have assumed that the axial current does not depend on somatic depolarization

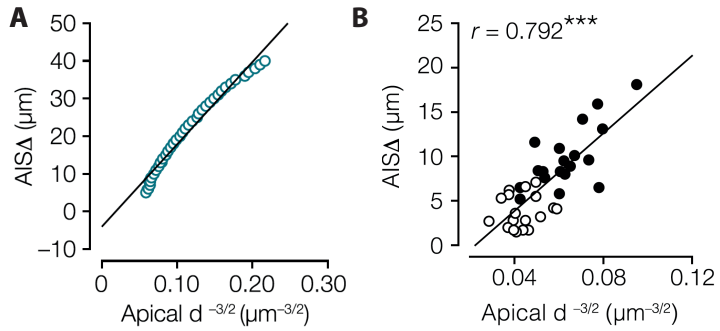

Figure 6.28: AIS position vs. dendrite diameter in cortical pyramidal cells (adapted from Hamada et al. (2016)). A, AIS position required to produce a constant depolarization speed at the soma in the model of Fig. 6.26, plotted vs. $d^{-1.5}$. B, AIS position vs. diameter d of the apical dendrite in layer 5 cortical pyramidal cells (note the different scales).

and therefore on dendritic properties, which is not exactly the case here for smaller diameters.

Thus, the current required to charge the soma scales theoretically as $d^{3/2}$. There is also an analytical formula for the impulse response of an isopotential soma plus cylindrical dendrite (the "ball-and-stick" model) (Rall, 1969; Tuckwell, 1988a) but it is not straightforward to estimate the dimensional scaling from it.

Thus, matching the axial current to the capacitance of a cylindrical somatodendritic process requires the following scaling:

$$x = \alpha d_{\text{dendrite}}^{-3/2} - \delta$$

where α is a proportionality factor. Fig. 6.28A shows in the two-cylinder model the AIS position that must be chosen in order to produce a fixed value for the somatic depolarization speed, for different values of dendrite diameter. Not that the scaling is not perfect (for the same reasons as above). Nonetheless, it qualitatively matches the measurements made on layer 5 pyramidal cells (Hamada et al., 2016), as shown on Fig. 6.28, which show as predicted an inverse correlation between AIS position and apical dendrite diameter, with a negative intercept and a slope with the correct order of magnitude. In those cells, dendritic diameter varies between 5 and 10 μ m and AIS position varies between nearly 0 and 20 μ m, but the first component of the somatic spike is not very variable. Thus the covariation between AIS position and dendrite diameter explains that the somatic spike is not very variable.

6.3.3 Spikelets

The previous discussion raises the possibility that axonal spikes fail to trigger a somatic spike. This is shown in Fig. 6.1C, where an axonal spike is initiated by current injection in the axon while the soma is hyperpolarized (also by current injection). The responses in the soma can be categorized in 3 different cases, depending on the initial membrane potential of the soma. If the soma is

Maybe a bit more on this, and simulations?

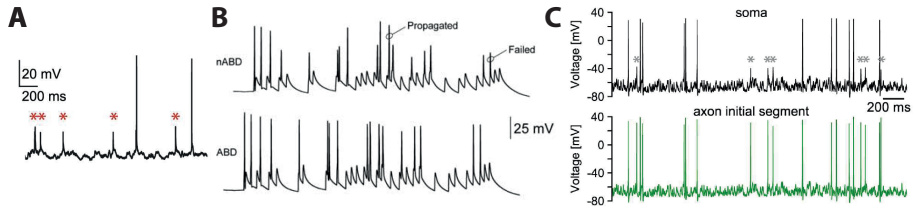

Figure 6.29: Spikelets. A, Spikelets observed in a hippocampal pyramidal neuron *in vivo*, shown with an asterisk (Epsztein et al., 2010). B, Spikelets observed in a dendrite of a dopaminergic neuron *in vitro* (top, "Failed"), matched to spikes in the axon (bottom; more precisely, the axon-bearing dendrite) (Gentet and Williams, 2007). C, Spikelets in the soma of a biophysical model of a pyramidal neuron (soma), matched to spikes in the AIS (bottom) (Michalikova et al., 2017).

at resting potential, a normal spike is seen at the soma. If the soma is hyperpolarized below some value, suddenly the normal spike is replaced by a smaller spike, which we call a "spikelet". The spikelet also has an all-or-none character: its amplitude does not change if the soma is further hyperpolarized, until it disappears below some threshold value. Below that value, somatic responses to the current injected at the axon look like passive responses.

These spikelets simply represent the passive response of the soma to the axonal spike, which is seen when that response does not reach the somatic spike threshold. Spikelets are observed *in vivo* (Fig. 6.29A, Epsztein et al. (2010)), although there are alternative explanations, such as gap junctions (a spike from another neuron is transmitted through the electrical synapse). They are also observed *in vitro* in dopaminergic neurons, in response to a train of simulated EPSPs (Fig. 6.29B, Gentet and Williams (2007)). In those neurons, the axon often originates not from the soma but from a dendrite. Fig. 6.29B shows that spikelets seen in the soma are matched to spikes in the axon-bearing dendrite; thus, spikelets correspond to failures of transmission to the soma. This phenomenon can be reproduced in a biophysical model of a cortical pyramidal cell (6.29C, Michalikova et al. (2017))[13].

How can the same neuron display both spikelets and full spikes? This can happen theoretically in two cases: 1) if the threshold for the somatic spike (for the second component of the spike) varies; 2) if the axial current transmitted to the soma at spike time varies. Different factors can modulate the threshold for the somatic spike, which we will examine in chapter **??**: the Na^+ channels can inactivate, due for example to a preceding spike; an outward conductance (e.g. K^+) may vary; and, for transient inputs, a current injected at the soma (or a synaptic current) can also modulate the threshold. The axial current can vary mainly if the available Na^+ conductance density varies, which can happen due to inactivation.

[13] In that model, the Na^+ channel density was reduced to increase the incidence of spikelets.

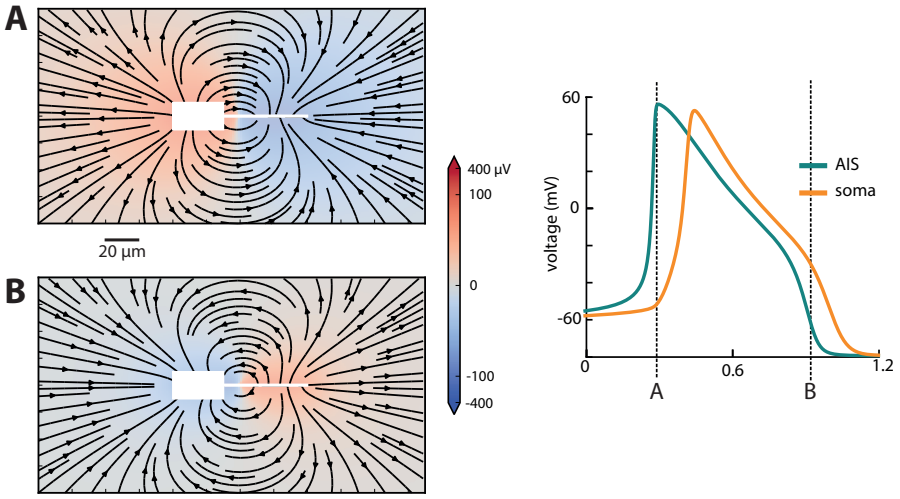

Figure 6.30: The soma-AIS dipole (adapted from Telenczuk et al. (2017)). Electrical potential (color) and field (arrows) produced by an action potential at the peak of the AIS spike (A) and during repolarization (B), in a two-cylinder biophysical model (white boxes).

6.4 Resistive coupling theory: extracellular signature of spikes

6.4.1 The dipole model

Figure 6.6 shows the circulation of current at spike initiation according to resistive theory: current enters the neuron at the AIS carried by Na^+ions, flows towards the soma, exits the neuron as capacitive current. The loop is closed by a resistive current in the extracellular medium (the resistivity is considered negligible). It is important to understand that this circulation diagram does not represent the propagation of the spike, but the current loop that sets up virtually instantaneously at spike initiation [14] — in an electrolyte, current is transmitted nearly at light speed [15]. This is why the term *backpropagation* often used to described the transmission of the axonal spike to the soma is slightly misleading, because the observed delay between the two action potentials corresponds mostly to the slower charging of the somatodendritic capacitance by the Na^+ current, rather than to the propagation of a wave (Telenczuk et al., 2017).

From an extracellular perspective, current simultaneously enters at the AIS and exits at the soma (and proximal dendrites). In electromagnetic theory, this is called an electric *dipole*. As discussed in section **??**, the extracellular potential $V_e(x)$ at a point $\mathbf{x}$ should then be:

$$V_e(\mathbf{x}) = \frac{I}{4\pi\sigma}\left(\frac{1}{|\mathbf{x}-\mathbf{x}_{\text{AIS}}|} - \frac{1}{|\mathbf{x}-\mathbf{x}_{\text{soma}}|}\right)$$

[14] This is correct in the ideal resistive model. More accurately, the speed is limited by the axonal capacitance.

[15] More precisely, $c/\sqrt{\epsilon}$, where c is light speed and ϵ is relative permittivity of the extracellular medium.

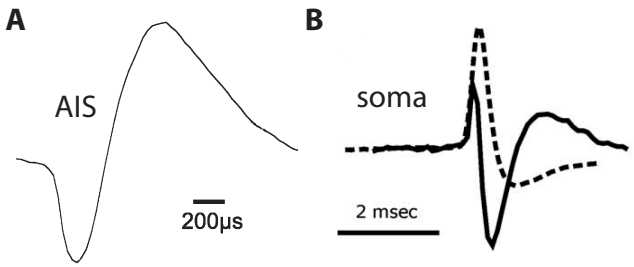

Figure 6.31: Extracellular spikes in layer 5 cortical neurons. A, Extracellular spike near the soma in a pyramidal cell (dashed) and an interneuron (solid) (**?**). B, Extracellular spike near the AIS of a pyramidal cell (Palmer and Stuart, 2006).

where σ is the conductivity of the extracellular medium (about $\sigma \approx 0.3$ S/m), $\mathbf{x}_{\text{AIS}}$ is the position of the initiation site, $\mathbf{x}_{\text{soma}}$ is the position of the soma and I is the current (axonal Na^+ current or equivalently somatodendritic capacitive current). Figure 6.30A shows the extracellular potential around a two-cylinder biophysical model (Telenczuk et al., 2017) at the time of the peak of the action potential in the distal AIS, which matches well the dipole model. The arrows represent the electrical field, which is the gradient of the potential, and corresponds to the circulation of current in the extracellular medium. As noted above, the extracellular potential develops fully over the spatial scale of the spike initiation system (AIS plus soma), before the spike can be observed in the somatic membrane potential. During repolarisation, the extracellular field reverses (Fig. 6.30B).

Thus, the soma and AIS simultaneously produce extracellular spikes of opposite polarity. Figure 6.31 shows extracellular spikes recorded near the AIS and soma of cortical neurons, which display this pattern.

6.4.2 Extracellular spike amplitude near the soma and AIS

How large is the extracellular spike near the soma and AIS? Close to a pole, the extracellular potential is dominated by the corresponding term:

$$V_e(\mathbf{x}) = \pm\frac{1}{4\pi\sigma}\frac{I}{|\mathbf{x}-\mathbf{x}_{\text{pole}}|}$$

We now consider that the measuring electrode is placed right next to the membrane. In the case of the axon, this means that the electrode is at distance $d_{\text{AIS}}/2$ of the pole, where d_{AIS} is the AIS diameter. In the case of the soma, if we assume that the pole is in the center of the soma (for example with a spherical soma), then the electrode is at distance $d_{\text{soma}}/2$ of the pole, where d_{soma} is the soma diameter. In summary, the potential is

$$V_e(\mathbf{x}) = \pm\frac{1}{2\pi\sigma}\frac{I}{d}$$

An important implication of this formula is that the extracellular signal measured near the soma is an order of magnitude smaller than the signal measured

near the AIS; specifically, by a ratio $d_{\text{soma}}/d_{\text{AIS}}$.

There are of courses important assumptions in this formula, namely that the electrode is at the point nearest to the pole; otherwise the measured potential would be smaller. For the AIS, the pole is near the distal end at spike initiation and near the proximal end at peak time of the axonal spike, as discussed in 6.2.5. We now examine these two cases.

At spike threshold

To simplify, let us assume that Na^+channels are clustered at a point in the axon, at distance x from the soma. Then at spike threshold, the Na^+current is k/R_a, where R_a is the coupling resistance (section 6.2.4). If we assume cylindrical geometry, then this resistance is:

$$R_a = \frac{4R_i}{\pi d_{\text{AIS}}^2} x$$

It follows that the extracellular potential is:

$$V_e(\text{AIS}) = \frac{k}{8\sigma R_i} \frac{d_{\text{AIS}}}{x}$$

With $\sigma \approx 0.3$ S/m, $R_i = 150$ Ω.cm, $d_{\text{AIS}} = 1.5$ μm, $k = 6$ mV, $x = 40$ μm, we obtain: $V_e(\text{AIS}) = 62$ μV.

At the soma, we would obtain:

$$V_e(\text{soma}) = -\frac{k}{8\sigma R_i} \frac{d_{\text{AIS}}^2}{x d_{\text{soma}}}$$

With $d_{\text{soma}} = 30$ μm, we would obtain $V_e(\text{soma}) = -3$ μV, which is very small.

At the peak of the axonal spike

Let us now examine the extracellular potential at the time of the peak of the axonal spike. This will be the maximum amplitude measured by the electrode. We have previously calculated the current transmitted to the soma, which in the resistive coupling model is the same as the Na^+current entering the AIS (section 6.3.1). A simple approximation is $I = \Delta V/R_a$, where $\Delta V \approx 100$ mV is the difference between somatic spike threshold and action potential peak. With that approximation, the extracellular potential is:

$$\begin{aligned} V_e(\text{AIS}) &= \frac{\Delta V}{8\sigma R_i} \frac{d_{\text{AIS}}}{x} \\ V_e(\text{soma}) &= -\frac{\Delta V}{8\sigma R_i} \frac{d_{\text{AIS}}^2}{x d_{\text{soma}}} \end{aligned}$$

Here x is the distance of proximal end of the AIS to the soma. With the same parameter values as above and $x = 10$ um, we obtain $V_e(\text{AIS}) \approx 4$ mV and $V_e(\text{soma}) \approx -200$ μV.

Using the more accurate formula for the current, x would be simply replaced by $x + \delta$, where δ depends on conductance density.

Scaling with neuron size

How does the extracellular spike scale with neuron size? If we assume that AIS position is tuned so as to produce a current that matches the somatic capacitance, then we simply have $I \propto d_{\text{soma}}^2$, and therefore:

$$\begin{aligned} V_e(\text{AIS}) &\propto \frac{d_{\text{soma}}^2}{d_{\text{AIS}}} \\ V_e(\text{soma}) &\propto d_{\text{soma}} \end{aligned}$$

Assuming that $d_{\text{AIS}} \propto d_{\text{soma}}^{3/2}$ or $d_{\text{soma}}^{4/3}$, we obtain $V_e(\text{AIS}) \propto \sqrt{d_{\text{soma}}}$ or $d_{\text{soma}}^{2/3}$.

6.4.3 Far-field approximation

We now examine the extracellular potential far from the soma and AIS. Let us consider a spherical soma of radius R, and an initiation site reduced to a point in the axon at distance Δ from the soma. Thus the distance between the two poles is $R + \Delta$, and the electrical reverts on a plane orthogonal to the axon at distance $(R + \Delta)/2$ of either pole, i.e., at distance $(\Delta - R)/2$ of the soma-axon junction. Far from that plane, the expression for the electric potential can be simplified as:

$$V_e(\mathbf{x}) \approx \frac{1}{4\pi\sigma} \frac{\mathbf{p} \cdot \hat{\mathbf{x}}}{|\mathbf{x}|^2}$$

where $\hat{\mathbf{x}} = \mathbf{x}/|\mathbf{x}|$ is the unit vector indicating the direction of the measurement point, and

$$\mathbf{p} = I(\mathbf{x}_{\text{AIS}} - \mathbf{x}_{\text{soma}})$$

Illustration? is called the *dipole moment*. Thus, far from the AIS, the electric potential scales as the square of distance. This scaling is well reproduced by a simulation of a two-cylinder model (**?**); it is more difficult to reproduce in a detailed biophysical model because it is masked by the forward and backward propagation of the action potential along the dendrites and axon.

6.4.4 The dipole moment

We now calculate the dipole moment at spike threshold and at peak time of the axonal spike.

At spike threshold

As before, we assume that Na^+channels are clustered at an axonal site at distance x from the soma, so that the Na^+current at threshold is $k/(r_a x)$. We now consider a spherical soma of diameter d_{soma}, so that the initiation site is at distance $x + d_{\text{soma}}/2$ of its center. Then the amplitude of the dipole moment is:

$$p = \frac{k}{r_a}\left(1 + \frac{d_{\text{soma}}}{2x}\right)$$

Thus, the dipole moment is roughly of order k/r_a. We note that this scales as d_a^2, where d_a is the axon diameter.

At the peak of the axonal spike

Let us now examine the dipole moment at the time of the peak of the axonal spike. With the approximation $I = \Delta V/(r_a x)$, the dipole moment is:

$$p = \frac{\Delta V}{r_a}\Big(1 + \frac{d_{\text{soma}}}{2x}\Big)$$

The more accurate formula is $I = \Delta V/(r_a(x+\delta))$, where δ depends on conductance density, which gives the following formula for the moment:

$$p = \frac{\Delta V}{r_a}.\frac{x + d_{\text{soma}}/2}{x+\delta}$$

The order of magnitude is thus $\Delta V/r_a$. With $\Delta V = 100$ mV and the same values for r_a as above, we get $p \approx 0.12$ pA.m. At a distance of 100 μm in the direction of the dipole axis, we then obtain $V_e \approx 3$ μV.

Scaling with neuron size

How does the dipole moment scale with neuron size? Let us assume that AIS position is tuned so as to produce a current that matches the somatic capacitance. We can first express the position as a function of I:

$$x + \delta = \frac{\Delta V}{r_a I}$$

Thus the dipole moment is:

$$p = I\Big(\frac{\Delta V}{r_a I} - \delta + d_{\text{soma}}/2\Big) = \frac{\Delta V}{r_a} + I(d_{\text{soma}}/2 - \delta)$$

We have the following scaling relations: $r_a \propto 1/d_{\text{AIS}}^2$, $\delta \propto \sqrt{d_{\text{AIS}}}$, $I \propto d_{\text{soma}}^2$, and $d_{\text{AIS}} \propto d_{\text{soma}}^{3/2}$ or $d_{\text{soma}}^{4/3}$. It follows that the overall scaling is $p \propto d_{\text{soma}}^3$.

6.5 Modulation of excitability by axonal currents

Research in progress.

6.6 Synapses on the initial segment

Research in progress.

6.7 Spike initiation in axons emerging from a dendrite

6.7.1 Axons emerging from a dendrite

In many neurons, the axon emerges not from the soma but from a dendrite (Fig. 6.32). This is in fact a relatively common situation in a variety of cell types

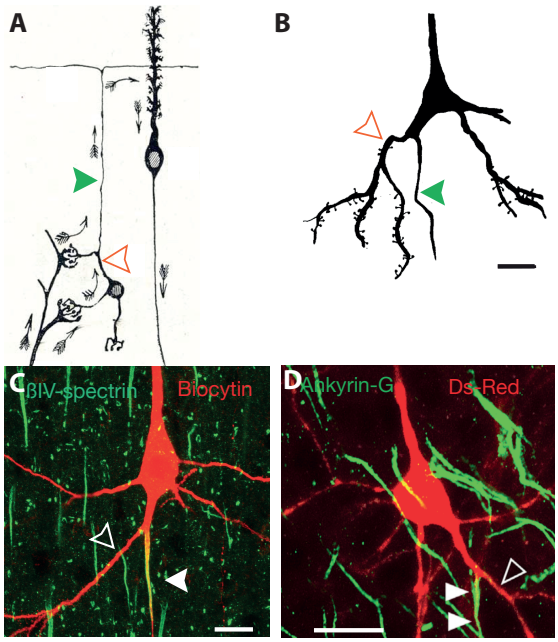

Figure 6.32: Axons emerging from a dendrite (adapted from Kole and Brette (2018)). Open arrows indicate the axon-carrying dendrite, close arrows indicate the axon. A, Cerebellar granule cell projecting to a Purkinje cell (right) (Ramon-y Cajal, 1899). B, Rat parietal cortex layer 2/3 pyramidal neuron (Peters, 1968). C, Rat layer 5 pyramidal neuron (AIS in green) (Hamada et al., 2016). D, Mouse hippocampal CA1 pyramidal neuron (AIS in green) (Thome et al., 2014).

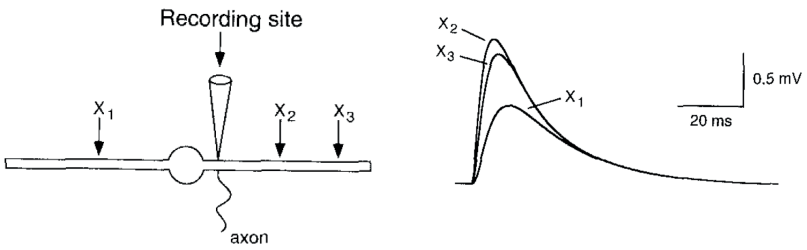

Figure 6.33: Postsynaptic potential at the axon start in a passive model, with an axon emerging from a dendrite, 50 μm from the soma. (Husser et al., 1995). The same current is injected at positions x_1, x_2 and x_3, and recorded at the start of the axon. Positions x_1 and x_2 are the same distance to the soma, while positions x_1 and x_3 are the same distance to the axon start.

(Kole and Brette, 2018), including 40% of cerebellar granule cells (Ramon-y Cajal, 1899; Houston et al., 2017), 75% of dopaminergic cells of the substantia nigra (Husser et al., 1995; Gentet and Williams, 2007; Blythe et al., 2009), 60% of the hippocampal pyramidal neurons, 30% of the thick-tufted somatosensory layer 5 pyramidal neurons, 40% of cortical interneuron basket cells and 60% of Martinotti cells (Hamada et al., 2016; Thome et al., 2014; Hfflin et al., 2017). The distance of the axon from the soma can be substantial, for example up to 40 μm in hippocampal pyramidal cells (Amaral, 1978; Thome et al., 2014), and even up to 260 μm in dopamingergic neurons (Husser et al., 1995; Gentet and Williams, 2007; Blythe et al., 2009).

According to resistive coupling theory[16], the soma acts as a current sink not only for the axonal initiation site, but also for any current injected in a proximal dendrite, in particular the dendrite that carries the axon. For this reason, synapses on the axon-bearing dendrite have a different impact on spike initiation than synapses on other dendrites.

6.7.2 Postsynaptic potential at the AIS

When a current I is injected in the axon-carrying dendrite, it flows towards the soma and thereby produces a voltage gradient between the soma and the injection point. Thus, the postsynaptic potential (PSP) V_d at the dendritic injection point is the PSP V_s observed at the soma plus a voltage gradient ΔV_d. Essentially the same PSP at the soma would be observed for a current injection in any dendrite of similar geometry, independently of whether it carries an axon. If the injection site is close the soma, then that PSP would also be essentially the same as if the current were injected directly in the soma.

The voltage gradient at the injection site is given by Ohm's law: $\Delta V_d = R_a I$, where R_a is the axial resistance from soma to injection point. In particular, it is roughly proportional to the distance of the injection point to the soma. What is the PSP at the AIS? Because little of that current is flowing to the axon, the potential at the AIS is essentially the same as the potential V_a at the axon start. We must then distinguish two cases.

Illustration maybe

[16] assuming it does apply to those cases, which may not be so clear when the AIS is very far from the soma.

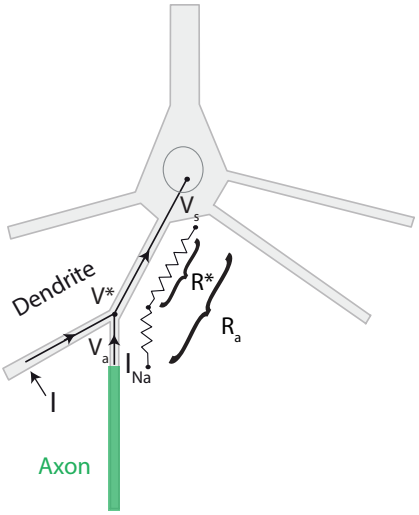

Figure 6.34: Stimulation of an axon-carrying dendrite (adapted from Kole and Brette (2018)).

If the current is injected between the soma and axon start, then the potential at the AIS would just equal the potential at the injection site: $V_a = V_d$. In particular, the PSP would be essentially proportional to the distance of the injection site (not of the axon) from the soma. If the current is injected in the dendrite beyond the axon start, then the potential at the AIS would equal $V_a = R_a^* I$, where R_a^* is the axial resistance between the soma and axon start. Thus in this case, the PSP at the AIS depends on the position of the axon, but not (much) on the position of the injection site.

This is illustrated in simulation in Fig. 6.33. Positions x_1 and x_2 are at the same distance from the soma, but injecting a synaptic current at x_2, on the axon-carrying dendrite, produces a much larger PSP at the axon start. Injecting a current at position x_3, which is about twice as far from the axon as position x_2, produces almost the same PSP at the axon start.

Thus, synapses placed on the axon-carrying dendrite produce a larger and more transient PSP at the AIS, and the magnitude of the extra voltage (compared to synapses on other dendrites) is determined by the position of the axon.

6.7.3 Excitability of an axon-bearing dendrite

These changes in PSP at the AIS transfer to changes in excitability. Consider a current I injected in an axon-bearing dendrite, beyond the branching point where the axon starts (Fig. 6.34). As we have seen previously, what matters is not so much the exact position of the stimulation point as the position of the axon. Let us denote R_a the axial coupling resistance between soma and AIS, and R^* the resistance between soma and axon start.

Applying Kirchoff's law at the branching point, we obtain:

$$I + I_{Na} = \frac{V^* - V_s}{R^*}$$

where V^* is the potential at the branching point (axon start). We deduce:

$$V^* = V_s + R^*(I + I_{Na})$$

We then match the Na^+current to the resistive current in the axon:

$$I_{Na} = \frac{V_a - V^*}{R_a - R^*}$$

We substitute the value of V^* obtained above, and after some algebra, we get:

$$I_{Na} = \frac{V_a - V_s - R^* I}{R_a}$$

This equation is the same as when the soma or a non-axon-bearing dendrite is stimulated, except V_s is replaced by $V_s + R^* I$. Thus, if the threshold for somatic stimulation is V_t, then a spike is produced when $V_s + R^* I$ reaches V_t, where V_s itself depends on I.

Thus, on a short time scale, if we stimulate the dendrite while the soma is at resting potential V_0, then the rheobase is

$$I^{\text{fast}}_{\text{rheobase}} = \frac{V_t - V_0}{R^*}$$

The rheobase is inversely proportional to the distance of the axon from the soma (importantly, not to the distance of the stimulation point).

On a longer time scale, let us assume $V_s = V_0 + R_m + I$, where R_m is the input resistance at the soma. Then the rheobase is

$$I^{\text{slow}}_{\text{rheobase}} = \frac{V_t - V_0}{R_m + R^*}$$

This corresponds to a negative shift in somatic threshold equals to

$$\Delta V_t = R^* I^{\text{slow}}_{\text{rheobase}} = \frac{R^*}{R_m + R^*}(V_t - V_0)$$

Thus, the somatic threshold appears lower when the axon-carrying dendrite is stimulated, by an amount that increases with the distance of the axon from the soma. This relation has been observed in hippocampal pyramidal neurons (Thome et al., 2014), as shown on Fig. 6.35.

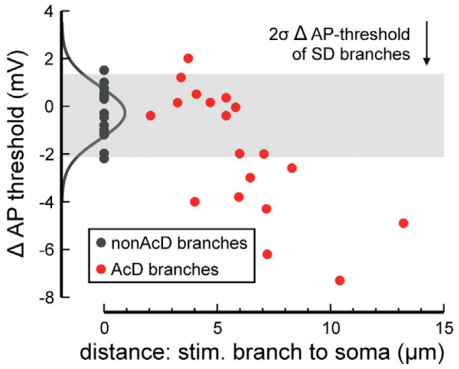

Figure 6.35: Somatic threshold when stimulating an axon-carrying dendrite (Thome et al., 2014). The points show the difference in somatic threshold for dendritic vs. somatic stimulation, as a function of distance of the axon from the soma (and in black: for non-axon-carrying dendrites).

Bibliography

Adrian, R. H. and Peachey, L. D. (1973). Reconstruction of the action potential of frog sartorius muscle. *The Journal of Physiology*, 235(1):103–131.

Amaral, D. G. (1978). A Golgi study of cell types in the hilar region of the hippocampus in the rat. *The Journal of Comparative Neurology*, 182(4 Pt 2):851–914.

Anderson, P. A. and Schwab, W. E. (1983). Action potential in neurons of motor nerve net of Cyanea (Coelenterata). *Journal of Neurophysiology*, 50(3):671–683.

Angelino, E. and Brenner, M. P. (2007). Excitability constraints on voltage-gated sodium channels. *PLoS computational biology*, 3(9):1751–60.

Anishkin, A., Loukin, S. H., Teng, J., and Kung, C. (2014). Feeling the hidden mechanical forces in lipid bilayer is an original sense. *Proceedings of the National Academy of Sciences*, 111(22):7898–7905.

Armstrong, C. M. (2007). Life among the axons. *Annual Review of Physiology*, 69:1–18.

Armstrong, C. M. and Bezanilla, F. (1977). Inactivation of the sodium channel. II. Gating current experiments. *The Journal of General Physiology*, 70(5):567–590.

Arsiero, M., Lscher, H.-R., Lundstrom, B. N., and Giugliano, M. (2007). The Impact of Input Fluctuations on the FrequencyCurrent Relationships of Layer 5 Pyramidal Neurons in the Rat Medial Prefrontal Cortex. *Journal of Neuroscience*, 27(12):3274–3284.

Astman, N., Gutnick, M. J., and Fleidervish, I. A. (1998). Activation of Protein Kinase C Increases Neuronal Excitability by Regulating Persistent Na+ Current in Mouse Neocortical Slices. *Journal of Neurophysiology*, 80(3):1547–1551.

Astman, N., Gutnick, M. J., and Fleidervish, I. A. (2006). Persistent sodium current in layer 5 neocortical neurons is primarily generated in the proximal axon. *The Journal of Neuroscience: The Official Journal of the Society for Neuroscience*, 26(13):3465–3473.

Astrm, K. J. and Murray, R. M. (2008). *Feedback Systems: An Introduction for Scientists and Engineers*. Princeton University Press, Princeton.

Attwell, D. and Laughlin, S. B. (2001). An Energy Budget for Signaling in the Grey Matter of the Brain. *Journal of Cerebral Blood Flow & Metabolism*, 21:1133–1145.

Azouz, R. and Gray, C. M. (1999). Cellular mechanisms contributing to response variability of cortical neurons in vivo. *J Neurosci*, 19(6):2209–23. undefined Mar 15 Cellular mechanisms contributing to response variability of cortical neurons in vivo 10066274 0270-6474 Journal Article

http://www.ncbi.nlm.nih.gov/entrez/query.fcgi?cmd=Retrieve&db=PubMed&dopt=Citation&list_uids=100
The Center for Neuroscience, Physiology, and Behavior, University of California, Davis, California 95616, USA.

Badel, L., Lefort, S., Brette, R., Petersen, C. C. H., Gerstner, W., and Richardson, M. J. E. (2008). Dynamic I-V curves are reliable predictors of naturalistic pyramidal-neuron voltage traces. *Journal of Neurophysiology*, 99(2):656–66.

Bahrey, H. L. P. and Moody, W. J. (2003). Early Development of Voltage-Gated Ion Currents and Firing Properties in Neurons of the Mouse Cerebral Cortex. *Journal of Neurophysiology*, 89(4):1761–1773.

Baker, P. F., Hodgkin, A. L., and Ridgway, E. B. (1971). Depolarization and calcium entry in squid giant axons. *The Journal of Physiology*, 218(3):709–755.

Bal, T. and Destexhe, A., editors (2009). *Dynamic-Clamp*. Springer US, New York, NY.

Baranauskas, G., David, Y., and Fleidervish, I. A. (2013). Spatial mismatch between the Na+ flux and spike initiation in axon initial segment. *Proceedings of the National Academy of Sciences*, 110(10):4051–4056.

Baranauskas, G. and Martina, M. (2006). Sodium Currents Activate without a Hodgkin and Huxley-Type Delay in Central Mammalian Neurons. *Journal of Neuroscience*, 26(2):671–684.

Baranauskas, G., Mukovskiy, A., Wolf, F., and Volgushev, M. (2010). The determinants of the onset dynamics of action potentials in a computational model. *Neuroscience*, 167(4):1070–1090.

Barrett, J. N. and Crill, W. E. (1980). Voltage clamp of cat motoneurone somata: properties of the fast inward current. *The Journal of Physiology*, 304(1):231–249.

Bender, K. J. and Trussell, L. O. (2012). The Physiology of the Axon Initial Segment. *Annual Review of Neuroscience*, 35(1):249–265.

Berg, H. C. (1975). Bacterial behaviour. *Nature*, 254(5499):389–392.

Berg, H. C. and Brown, D. A. (1972). Chemotaxis in Escherichia coli analysed by Three-dimensional Tracking. *Nature*, 239(5374):500–504.

Bernstein, J. (1868). Ueber den zeitlichen Verlauf der negativen Schwankung des Nervenstroms. *Pflgers Archiv European Journal of Physiology*, 1(1):173–207.

Bernstein, J. (1912). *Elektrobiologie*. Die Wissenschaft,, 44 Hft, Wissenschaft, Braunschweig.

Bezanilla, F. and Armstrong, C. (1977). Inactivation of the sodium channel. I. Sodium current experiments. *The Journal of General Physiology*, 70(5):549–566.

Binggeli, R. and Weinstein, R. C. (1986). Membrane potentials and sodium channels: Hypotheses for growth regulation and cancer formation based on changes in sodium channels and gap junctions. *Journal of Theoretical Biology*, 123(4):377–401.

Blythe, S. N., Wokosin, D., Atherton, J. F., and Bevan, M. D. (2009). Cellular Mechanisms Underlying Burst Firing in Substantia Nigra Dopamine Neurons. *Journal of Neuroscience*, 29(49):15531–15541.

Boiko, T., Van Wart, A., Caldwell, J. H., Levinson, S. R., Trimmer, J. S., and Matthews, G. (2003). Functional specialization of the axon initial segment by isoform-specific sodium channel targeting. *The Journal of Neuroscience: The Official Journal of the Society for Neuroscience*, 23(6):2306–2313.

Boyle, P. J. and Conway, E. J. (1941). Potassium accumulation in muscle and associated changes. *The Journal of Physiology*, 100(1):1–63.

Brehm, P., Dunlap, K., and Eckert, R. (1978). Calcium-dependent repolarization in Paramecium. *The Journal of Physiology*, 274:639–654.

Brehm, P. and Eckert, R. (1978). Calcium entry leads to inactivation of calcium channel in Paramecium. *Science*, 202(4373):1203–1206.

Brehm, P., Eckert, R., and Tillotson, D. (1980). Calcium-mediated inactivation of calcium current in Paramecium. *The Journal of Physiology*, 306:193–203.

Brennecke, R. and Lindemann, B. (1974). Design of a fast voltage clamp for biological membranes, using discontinuous feedback. *Rev Sci Instrum*, 45(5):656–61. undefined May Design of a fast voltage clamp for biological membranes, using discontinuous feedback 4826158 0034-6748 Journal Article http://www.ncbi.nlm.nih.gov/entrez/query.fcgi?cmd=Retrieve&db=PubMed&dopt=Citation&list_uids=4826158.

Brette, R. (2013). Sharpness of Spike Initiation in Neurons Explained by Compartmentalization. *PLoS Comput Biol*, 9(12):e1003338.

Brette, R. (2015). What is the most realistic single-compartment model of spike initiation? *PLoS computational biology*, 11(4):e1004114.

Brette, R. and Destexhe, A. (2012). Intracellular recording. In *Handbook of neural activity measurement*. Cambridge University Press.

Brette, R. and Gerstner, W. (2005). Adaptive exponential integrate-and-fire model as an effective description of neuronal activity. *Journal of Neurophysiology*, 94(5):3637–42.

Brette, R., Piwkowska, Z., Monier, C., Rudolph-Lilith, M., Fournier, J., Levy, M., Frgnac, Y., Bal, T., and Destexhe, A. (2008). High-resolution intracellular recordings using a real-time computational model of the electrode. *Neuron*, 59(3):379–91.

BROCK, L. G., COOMBS, J. S., and ECCLES, J. C. (1952). The recording of potentials from motoneurones with an intracellular electrode. *The Journal of Physiology*, 117(4):431–460.

Brunel, N., Chance, F. S., Fourcaud, N., and Abbott, L. F. (2001). Effects of synaptic noise and filtering on the frequency response of spiking neurons. *Phys.rev.lett.*, 86(10):2186. undefined Effects of synaptic noise and filtering on the frequency response of spiking neurons 985 DA - 20010406 NOT IN FILE PM:11289886 LPS, Ecole Normale Superieure, Paris, France.

Carter, B. C. and Bean, B. P. (2009). Sodium entry during action potentials of mammalian central neurons: incomplete inactivation and reduced metabolic efficiency in fast-spiking neurons. *Neuron*, 64(6):898–909.

Chen, Y., Yu, F. H., Sharp, E. M., Beacham, D., Scheuer, T., and Catterall, W. A. (2008). Functional properties and differential neuromodulation of Nav1.6 channels. *Molecular and Cellular Neuroscience*, 38(4):607–615.

Clay, J. R. (1991). A paradox concerning ion permeation of the delayed rectifier potassium ion channel in squid giant axons. *The Journal of Physiology*, 444:499–511.

Clay, J. R. (2005). Axonal excitability revisited. *Progress in Biophysics and Molecular Biology*, 88(1):59–90.

Colbert, C. M. and Johnston, D. (1996). Axonal Action-Potential Initiation and Na+ Channel Densities in the Soma and Axon Initial Segment of Subicular Pyramidal Neurons. *The Journal of Neuroscience*, 16(21):6676–6686.

Colbert, C. M. and Pan, E. (2002). Ion channel properties underlying axonal action potential initiation in pyramidal neurons. *Nat Neurosci*, 5(6):533–538.

Cole, K. S. (1949). Dynamic electrical characteristics of the squid axon membrane. *Arch. Sci. Physiol*, 3(25):3–25.

Cole, K. S. and Curtis, H. J. (1938). Electric Impedance of Nitella During Activity. *The Journal of General Physiology*, 22(1):37–64.

Cole, K. S. and Curtis, H. J. (1939). ELECTRIC IMPEDANCE OF THE SQUID GIANT AXON DURING ACTIVITY. *The Journal of General Physiology*, 22(5):649–670.

Cole, K. S. and Moore, J. W. (1960). Potassium Ion Current in the Squid Giant Axon. *Biophysical Journal*, 1(1):1–14.

Coombs, J. S., Curtis, D. R., and Eccles, J. C. (1957a). The generation of impulses in motoneurones. *The Journal of Physiology*, 139(2):232–249.

Coombs, J. S., Curtis, D. R., and Eccles, J. C. (1957b). The interpretation of spike potentials of motoneurones. *The Journal of Physiology*, 139(2):198–231.

Cotel, F., Exley, R., Cragg, S. J., and Perrier, J.-F. (2013). Serotonin spillover onto the axon initial segment of motoneurons induces central fatigue by inhibiting action potential initiation. *Proceedings of the National Academy of Sciences of the United States of America*, 110(12):4774–4779.

De Loof, A. (1986). The electrical dimension of cells: the cell as a miniature electrophoresis chamber. *International Review of Cytology*, 104:251–352.

Debanne, D., Bialowas, A., and Rama, S. (2013). What are the mechanisms for analogue and digital signalling in the brain? *Nature Reviews Neuroscience*, 14(1):63–69.

Debanne, D., Campanac, E., Bialowas, A., Carlier, E., and Alcaraz, G. (2011). Axon Physiology. *Physiological Reviews*, 91(2):555–602.

Dekker, J. P. and Yellen, G. (2006). Cooperative gating between single HCN pacemaker channels. *The Journal of general physiology*, 128(5):561–567.

Diwakar, S., Magistretti, J., Goldfarb, M., Naldi, G., and D'Angelo, E. (2009). Axonal Na+ Channels Ensure Fast Spike Activation and Back-Propagation in Cerebellar Granule Cells. *Journal of Neurophysiology*, 101(2):519–532.

Dodge, F. A. and Frankenhaeuser, B. (1959). Sodium currents in the myelinated nerve fibre of Xenopus laevis investigated with the voltage clamp technique. *The Journal of Physiology*, 148(1):188–200.

Dreosti, E., Esposti, F., Baden, T., and Lagnado, L. (2011). In vivo evidence that retinal bipolar cells generate spikes modulated by light. *Nature neuroscience*, 14(8):951–952.

Eckert, R. (1972). Bioelectric Control of Ciliary Activity. *Science*, 176(4034):473–481.

Eckert, R. and Brehm, P. (1979). Ionic mechanisms of excitation in Paramecium. *Annual Review of Biophysics and Bioengineering*, 8:353–383.

Eckert, R. and Chad, J. E. (1984). Inactivation of Ca channels. *Progress in Biophysics and Molecular Biology*, 44(3):215–267.

Eckert, R. and Naitoh, Y. (1970). Passive electrical properties of Paramecium and problems of ciliary coordination. *The Journal of General Physiology*, 55(4):467–483.

Eckert, R. and Sibaoka, T. (1968). The Flash-Triggering Action Potential of the Luminescent Dinoflagellate Noctiluca. *The Journal of General Physiology*, 52(2):258–282.

Einevoll, G. T., Kayser, C., Logothetis, N. K., and Panzeri, S. (2013). Modelling and analysis of local field potentials for studying the function of cortical circuits. *Nature Reviews. Neuroscience*, 14(11):770–785.

El Hady, A. and Machta, B. B. (2015). Mechanical surface waves accompany action potential propagation. *Nature Communications*, 6:6697.

Emiliani, V., Cohen, A. E., Deisseroth, K., and Husser, M. (2015). All-Optical Interrogation of Neural Circuits. *The Journal of Neuroscience: The Official Journal of the Society for Neuroscience*, 35(41):13917–13926.

Epsztein, J., Lee, A. K., Chorev, E., and Brecht, M. (2010). Impact of Spikelets on Hippocampal CA1 Pyramidal Cell Activity During Spatial Exploration. *Science*, 327(5964):474–477.

Faisal, A. A., White, J. A., and Laughlin, S. B. (2005). Ion-Channel Noise Places Limits on the Miniaturization of the Brains Wiring. *Current Biology*, 15(12):1143–1149.

Fatt, P. (1957). Sequence of events in synaptic activation of a motoneurone. *Journal of Neurophysiology*, 20(1):61–80.

Febvre-Chevalier, C., Bilbaut, A., Bone, Q., and Febvre, J. (1986). Sodium-Calcium Action Potential Associated with Contraction in the Heliozoan Actinocoryne Contractilis. *Journal of Experimental Biology*, 122(1):177–192.

Feyerabend, P. (2010). *Against method*. Verso, London.

Fleidervish, I. A., Lasser-Ross, N., Gutnick, M. J., and Ross, W. N. (2010). Na+ imaging reveals little difference in action potential-evoked Na+ influx between axon and soma. *Nat Neurosci*, 13(7):852–860.

Fourcaud-Trocme, N., Hansel, D., van Vreeswijk, C., and Brunel, N. (2003). How spike generation mechanisms determine the neuronal response to fluctuating inputs. *J neurosci*, 23(37):11628–40. undefined Dec 17 How spike generation mechanisms determine the neuronal response to fluctuating inputs 14684865 1529-2401 Journal Article http://www.ncbi.nlm.nih.gov/entrez/query.fcgi?cmd=Retrieve&db=PubMed&dopt=Citation&list_uids=14684865 Centre National de la Recherche Scientifique Unite Mixte de Recherche 8119, Neurophysique et Physiologie du Systeme Moteur, Unite de Formation et de Recherche Biomedicale, Universite Paris 5 Rene Descartes, 75270 Paris Cedex 06, France.

Frankenhaeuser, B. (1960). Sodium permeability in toad nerve and in squid nerve. *The Journal of Physiology*, 152(1):159–166.

Galvani, L. (1791). De viribus electricitatis in motu musculari: Commentarius. *Bologna: Tip. Istituto delle Scienze, 1791; 58 p.: 4 tavv. ft; in 4.; DCC. f. 70.*

Gentet, L. J., Stuart, G. J., and Clements, J. D. (2000). Direct measurement of specific membrane capacitance in neurons. *Biophysical Journal*, 79(1):314–320.

Gentet, L. J. and Williams, S. R. (2007). Dopamine gates action potential backpropagation in midbrain dopaminergic neurons. *The Journal of Neuroscience: The Official Journal of the Society for Neuroscience*, 27(8):1892–1901.

Gerstner, W. and Naud, R. (2009). How Good Are Neuron Models? *Science*, 326(5951):379–380.

Gilly, W. F. and Armstrong, C. M. (1984). Threshold channels–a novel type of sodium channel in squid giant axon. *Nature*, 309(5967):448–450.

Goldman, D. E. (1943). Potential, Impedance, and Rectification in Membranes. *The Journal of General Physiology*, 27(1):37–60.

Goodman, C. S. and Spitzer, N. C. (1981). The development of electrical properties of identified neurones in grasshopper embryos. *The Journal of Physiology*, 313:385–403.

Hagiwara, S., Naka, K.-i., and Chichibu, S. (1964). Membrane Properties of Barnacle Muscle Fiber. *Science*, 143(3613):1446–1448.

Hallermann, S., de Kock, C. P. J., Stuart, G. J., and Kole, M. H. P. (2012). State and location dependence of action potential metabolic cost in cortical pyramidal neurons. *Nature Neuroscience*, 15(7):1007–1014.

Hamada, M. S., Goethals, S., de Vries, S. I., Brette, R., and Kole, M. H. P. (2016). Covariation of axon initial segment location and dendritic tree normalizes the somatic action potential. *Proceedings of the National Academy of Sciences of the United States of America*, 113(51):14841–14846.

Harrison, P. M., Badel, L., Wall, M. J., and Richardson, M. J. E. (2015). Experimentally Verified Parameter Sets for Modelling Heterogeneous Neocortical Pyramidal-Cell Populations. *PLOS Computational Biology*, 11(8):e1004165.

Harz, H. and Hegemann, P. (1991). Rhodopsin-regulated calcium currents in Chlamydomonas. *Nature*, 351(6326):489–491.

Heflin, S. J. and Cook, P. B. (2007). Narrow and wide field amacrine cells fire action potentials in response to depolarization and light stimulation. *Visual Neuroscience*, 24(2):197–206.

Heimburg, T. and Jackson, A. D. (2005). On soliton propagation in biomembranes and nerves. *Proceedings of the National Academy of Sciences of the United States of America*, 102(28):9790–9795.

Hennessey, T. M. and Kung, C. (1984). An anticalmodulin drug, W-7, inhibits the voltage-dependent calcium current in Paramecium caudatum. *Journal of Experimental Biology*, 110(1):169–181.

Henze, D. A. and Buzsaki, G. (2001). Action potential threshold of hippocampal pyramidal cells in vivo is increased by recent spiking activity. *Neuroscience*, 105(1):121–30. undefined Action potential threshold of hippocampal pyramidal cells in vivo is increased by recent spiking activity 11483306 0306-4522 Journal Article http://www.ncbi.nlm.nih.gov/entrez/query.fcgi?cmd=Retrieve&db=PubMed&dopt=Citation&list_uids=11483306 Center for Molecular and Behavioral Neuroscience, Rutgers, The State University of New Jersey, 197 University Avenue, Newark, NJ 07102, USA.

Herndon, R. M. (1963). The fine structure of the Purkinje cell. *The Journal of Cell Biology*, 18(1):167–180.

Hill, B. C., Schubert, E. D., Nokes, M. A., and Michelson, R. P. (1977). Laser interferometer measurement of changes in crayfish axon diameter concurrent with action potential. *Science*, 196(4288):426–428.

Hille, B. (2001). *Ion Channels of Excitable Membranes*. Sinauer Associates. undefined 3rd Edition Ion Channels of Excitable Membranes.

Hodgkin, A. (1975). The optimum density of sodium channels in an unmyelinated nerve. *Philosophical Transactions of the Royal Society of London. Series B, Biological Sciences*, 270(908):297–300.

Hodgkin, A. and Huxley, A. (1939). Action Potentials Recorded from Inside a Nerve Fibre. *Nature*, 144(3651):710.

Hodgkin, A. and Huxley, A. (1952a). A quantitative description of membrane current and its application to conduction and excitation in nerve. *J Physiol (Lond)*, 117:500.

Hodgkin, A. L. (1939). The relation between conduction velocity and the electrical resistance outside a nerve fibre. *The Journal of Physiology*, 94(4):560–570.

Hodgkin, A. L. (1951). The Ionic Basis of Electrical Activity in Nerve and Muscle. *Biological Reviews*, 26(4):339–409.

Hodgkin, A. L. (1964). *The conduction of the nervous impulse*. C. C. Thomas.

Hodgkin, A. L. and Huxley, A. F. (1952b). The components of membrane conductance in the giant axon of Loligo. *The Journal of Physiology*, 116(4):473–496.

Hodgkin, A. L. and Huxley, A. F. (1952c). Currents carried by sodium and potassium ions through the membrane of the giant axon of Loligo. *The Journal of Physiology*, 116(4):449–472.

Hodgkin, A. L. and Huxley, A. F. (1952d). The dual effect of membrane potential on sodium conductance in the giant axon of Loligo. *The Journal of Physiology*, 116(4):497–506.

Hodgkin, A. L. and Huxley, A. F. (1953). Movement of radioactive potassium and membrane current in a giant axon. *The Journal of Physiology*, 121(2):403–414.

Hodgkin, A. L., Huxley, A. F., and Katz, B. (1952). Measurement of current-voltage relations in the membrane of the giant axon of Loligo. *The Journal of Physiology*, 116(4):424–448.

Hodgkin, A. L. and Katz, B. (1949). The effect of sodium ions on the electrical activity of the giant axon of the squid. *The Journal of Physiology*, 108(1):37.

Hodgkin, A. L. and Keynes, R. D. (1953). The mobility and diffusion coefficient of potassium in giant axons from Sepia. *The Journal of Physiology*, 119(4):513–528.

Hook, C. and Hildebrand, E. (1979). Excitation of paramecium. *Journal of Mathematical Biology*, 8(2):197–214.

Hoppensteadt, F. C. and Peskin, C. (2004). *Modeling and Simulation in Medicine and the Life Sciences*. Springer, New York, 2nd edition edition.

Hossain, W. A., Antic, S. D., Yang, Y., Rasband, M. N., and Morest, D. K. (2005). Where is the spike generator of the cochlear nerve? Voltage-gated sodium channels in the mouse cochlea. *The Journal of Neuroscience: The Official Journal of the Society for Neuroscience*, 25(29):6857–68.

Houston, C. M., Diamanti, E., Diamantaki, M., Kutsarova, E., Cook, A., Sultan, F., and Brickley, S. G. (2017). Exploring the significance of morphological diversity for cerebellar granule cell excitability. *Scientific Reports*, 7:46147.

Howarth, C., Gleeson, P., and Attwell, D. (2012). Updated Energy Budgets for Neural Computation in the Neocortex and Cerebellum. *Journal of Cerebral Blood Flow & Metabolism*, 32(7):1222–1232.

Hoyt, R. C. (1963). THE SQUID GIANT AXON. MATHEMATICAL MODELS. *Biophysical Journal*, 3:399–431.

Hoyt, R. C. (1968). Sodium Inactivation in Nerve Fibers. *Biophysical Journal*, 8(10):1074–1097.

Hu, W., Tian, C., Li, T., Yang, M., Hou, H., and Shu, Y. (2009). Distinct contributions of Na(v)1.6 and Na(v)1.2 in action potential initiation and backpropagation. *Nature Neuroscience*, 12(8):996–1002.

Huxley, A. F. (1974). Muscular contraction. *The Journal of Physiology*, 243(1):1–43.

Husser, M., Stuart, G., Racca, C., and Sakmann, B. (1995). Axonal initiation and active dendritic propagation of action potentials in substantia nigra neurons. *Neuron*, 15(3):637–647.

Hfflin, F., Jack, A., Riedel, C., Mack-Bucher, J., Roos, J., Corcelli, C., Schultz, C., Wahle, P., and Engelhardt, M. (2017). Heterogeneity of the Axon Initial Segment in Interneurons and Pyramidal Cells of Rodent Visual Cortex. *Frontiers in Cellular Neuroscience*, 11:332.

Ilin, V., Malyshev, A., Wolf, F., and Volgushev, M. (2013). Fast Computations in Cortical Ensembles Require Rapid Initiation of Action Potentials. *The Journal of Neuroscience*, 33(6):2281–2292.

Inda, M. C., DeFelipe, J., and Muoz, A. (2006). Voltage-gated ion channels in the axon initial segment of human cortical pyramidal cells and their relationship with chandelier cells. *Proceedings of the National Academy of Sciences of the United States of America*, 103(8):2920–2925.

Jacobson, K., Sheets, E. D., and Simson, R. (1995). Revisiting the fluid mosaic model of membranes. *Science (New York, N.Y.)*, 268(5216):1441–1442.

Jennings, H. S. H. S. (1906). *Behavior of the lower organisms*. New York, The Columbia university press, The Macmillan company, agents; [etc., etc.].

Katz, B. and Miledi, R. (1970). Membrane Noise produced by Acetylcholine. *Nature*, 226(5249):962–963.

Kim, G. E., Kronengold, J., Barcia, G., Quraishi, I. H., Martin, H. C., Blair, E., Taylor, J. C., Dulac, O., Colleaux, L., Nabbout, R., and Kaczmarek, L. K. (2014). Human Slack Potassium Channel Mutations Increase Positive Cooperativity between Individual Channels. *Cell Reports*, 9(5):1661–1672.

Koch, C. (1999). *Biophysics of computation: Information processing in single neurons*. Oxford University Press, USA.

Koch, C., Bernander, O., and Douglas, R. J. (1995). Do neurons have a voltage or a current threshold for action potential initiation? *Journal of Computational Neuroscience*, 2(1):63–82.

Kole, M. H. and Brette, R. (2018). The electrical significance of axon location diversity. *Current Opinion in Neurobiology*, 51:52–59.

Kole, M. H. P., Ilschner, S. U., Kampa, B. M., Williams, S. R., Ruben, P. C., and Stuart, G. J. (2008). Action potential generation requires a high sodium channel density in the axon initial segment. *Nature Neuroscience*, 11(2):178–186.

Kole, M. H. P., Letzkus, J. J., and Stuart, G. J. (2007). Axon initial segment Kv1 channels control axonal action potential waveform and synaptic efficacy. *Neuron*, 55(4):633–647.

Kole, M. H. P. and Stuart, G. J. (2008). Is action potential threshold lowest in the axon? *Nat Neurosci*, 11(11):1253–1255.

Kosaka, T. (1980). The axon initial segment as a synaptic site: Ultrastructure and synaptology of the initial segment of the pyramidal cell in the rat hippocampus (CA3 region). *Journal of Neurocytology*, 9(6):861–882.

Kralj, J. M., Hochbaum, D. R., Douglass, A. D., and Cohen, A. E. (2011). Electrical Spiking in Escherichia coli Probed with a Fluorescent Voltage-Indicating Protein. *Science*, 333(6040):345–348.

Kramer, E. M. and Myers, D. R. (2013). Osmosis is not driven by water dilution. *Trends in Plant Science*, 18(4):195–197.

Kress, G. J., Dowling, M. J., Eisenman, L. N., and Mennerick, S. (2010). Axonal sodium channel distribution shapes the depolarized action potential threshold of dentate granule neurons. *Hippocampus*, 20(4):558–571.

Kress, G. J., Dowling, M. J., Meeks, J. P., and Mennerick, S. (2008). High Threshold, Proximal Initiation, and Slow Conduction Velocity of Action Potentials in Dentate Granule Neuron Mossy Fibers. *Journal of Neurophysiology*, 100(1):281–291.

Kuhn, T. S. (1962). *The structure of scientific revolutions*. The University of Chicago Press, Chicago.

Kung, C. and Eckert, R. (1972). Genetic Modification of Electric Properties in an Excitable Membrane. *Proceedings of the National Academy of Sciences*, 69(1):93–97.

Kushmerick, M. J. and Podolsky, R. J. (1969). Ionic mobility in muscle cells. *Science (New York, N.Y.)*, 166(3910):1297–1298.

Lakatos, I. (1976). Falsification and the Methodology of Scientific Research Programmes. In Harding, S. G., editor, *Can Theories be Refuted?*, number 81 in Synthese Library, pages 205–259. Springer Netherlands.

Lapicque, L. (1907). Recherches quantitatives sur l'excitation lectrique des nerfs traite comme une polarisation. *J physiol pathol gen*, 9:620–635. undefined Recherches quantitatives sur l'excitation lectrique des nerfs traite comme une polarisation J physiol pathol gen.

Leterrier, C. and Dargent, B. (2014). No Pasaran! Role of the axon initial segment in the regulation of protein transport and the maintenance of axonal identity. *Seminars in Cell & Developmental Biology*, 27:44–51.

Leterrier, C., Potier, J., Caillol, G., Debarnot, C., RuedaBoroni, F., and Dargent, B. (2015). Nanoscale Architecture of the Axon Initial Segment Reveals an Organized and Robust Scaffold. *Cell Reports*, 13(12):2781–2793.

Levin, M. (2014). Molecular bioelectricity: how endogenous voltage potentials control cell behavior and instruct pattern regulation in vivo. *Molecular Biology of the Cell*, 25(24):3835–3850.

Levitan, I. B. (1994). Modulation of ION Channels by Protein Phosphorylation and Dephosphorylation. *Annual Review of Physiology*, 56(1):193–212.

Leys, S. P., Mackie, G. O., and Meech, R. W. (1999). Impulse conduction in a sponge. *Journal of Experimental Biology*, 202(9):1139–1150.

LING, G. and GERARD, R. W. (1949). The normal membrane potential of frog sartorius fibers. *Journal of Cellular Physiology*, 34(3):383–96.

Ling, G. N. (1962). *A physical theory of the living state: The association-induction hypothesis; with considerations of the mechanics involved in ionic specificity*. Blaisdell Pub. Co, 1st edition edition.

Lorincz, A. and Nusser, Z. (2010). Molecular Identity of Dendritic Voltage-Gated Sodium Channels. *Science*, 328(5980):906–909.

Luo, C. H. and Rudy, Y. (1991). A model of the ventricular cardiac action potential. Depolarization, repolarization, and their interaction. *Circulation Research*, 68(6):1501–1526.

Machemer, H. (1998). Electrophysiology. In Grtz, P. D. H.-D., editor, *Paramecium*, pages 185–215. Springer Berlin Heidelberg.

Machemer, H. and Eckert, R. (1973). Electrophysiological control of reversed ciliary beating in Paramecium. *The Journal of General Physiology*, 61(5):572–587.

Machemer, H. and Ogura, A. (1979). Ionic conductances of membranes in ciliated and deciliated Paramecium. *The Journal of Physiology*, 296:49–60.

Madeja, M. (2000). Do neurons have a reserve of sodium channels for the generation of action potentials? A study on acutely isolated CA1 neurons from the guinea-pig hippocampus. *European Journal of Neuroscience*, 12(1):1–7.

Magee, J. C. and Johnston, D. (1995). Characterization of single voltage-gated Na+ and Ca2+ channels in apical dendrites of rat CA1 pyramidal neurons. *The Journal of Physiology*, 487(Pt 1):67–90.

Manwani, A. and Koch, C. (1999). Detecting and Estimating Signals in Noisy Cable Structures, I: Neuronal Noise Sources. *Neural Computation*, 11(8):1797–1829.

Marmont, G. (1949). Studies on the axon membrane; a new method. *J Cell Physiol*, 34(3):351–82.

Marx, S. O., Gaburjakova, J., Gaburjakova, M., Henrikson, C., Ondrias, K., and Marks, A. R. (2001). Coupled gating between cardiac calcium release channels (ryanodine receptors). *Circulation research*, 88(11):1151–1158.

Marx, S. O., Ondrias, K., and Marks, A. R. (1998). Coupled gating between individual skeletal muscle Ca2+ release channels (ryanodine receptors). *Science (New York, N.Y.)*, 281(5378):818–821.

Masi, E., Ciszak, M., Santopolo, L., Frascella, A., Giovannetti, L., Marchi, E., Viti, C., and Mancuso, S. (2015). Electrical spiking in bacterial biofilms. *Journal of the Royal Society, Interface / the Royal Society*, 12(102):20141036.

McLaughlin, S. (1977). Electrostatic Potentials at Membrane-Solution Interfaces. In Kleinzeller, F. B. a. A., editor, *Current Topics in Membranes and Transport*, volume 9, pages 71–144. Academic Press.

Meeks, J. P. and Mennerick, S. (2007). Action potential initiation and propagation in CA3 pyramidal axons. *Journal of Neurophysiology*, 97(5):3460–3472.

Meisel, C., Klaus, A., Kuehn, C., and Plenz, D. (2015). Critical Slowing Down Governs the Transition to Neuron Spiking. *PLoS Comput Biol*, 11(2):e1004097.

Michalikova, M., Remme, M. W. H., and Kempter, R. (2017). Spikelets in Pyramidal Neurons: Action Potentials Initiated in the Axon Initial Segment That Do Not Activate the Soma. *PLOS Computational Biology*, 13(1):e1005237.

Milescu, L. S., Bean, B. P., and Smith, J. C. (2010). Isolation of Somatic Na+ Currents by Selective Inactivation of Axonal Channels with a Voltage Prepulse. *The Journal of Neuroscience*, 30(22):7740–7748.

Misonou, H., Mohapatra, D. P., Park, E. W., Leung, V., Zhen, D., Misonou, K., Anderson, A. E., and Trimmer, J. S. (2004). Regulation of ion channel localization and phosphorylation by neuronal activity. *Nature Neuroscience*, 7(7):711–718.

Molina, M. L., Barrera, F. N., Fernndez, A. M., Poveda, J. A., Renart, M. L., Encinar, J. A., Riquelme, G., and Gonzlez-Ros, J. M. (2006). Clustering and coupled gating modulate the activity in KcsA, a potassium channel model. *The Journal of biological chemistry*, 281(27):18837–18848.

Molleman, A. (2002). *Patch Clamping: An Introductory Guide to Patch Clamp Electrophysiology*. Wiley-Blackwell, New York.

Morris, C. and Lecar, H. (1981). Voltage oscillations in the barnacle giant muscle fiber. *Biophysical Journal*, 35(1):193–213.

Nagumo, J. S., Arimoto, S., and Yoshizawa, S. (1962). An active pulse transmission line simulating nerve axon. volume 50, pages 2061–2071. undefined Proc. IRE An active pulse transmission line simulating nerve axon.

Naitoh, Y. and Eckert, R. (1968). Electrical properties of Paramecium caudatum: all-or-none electrogenesis. *Zeitschrift fr vergleichende Physiologie*, 61(4):453–472.

Naitoh, Y. and Eckert, R. (1973). Sensory Mechanisms in Paramecium. *Journal of Experimental Biology*, 59(1):53–65.

Naitoh, Y., Eckert, R., and Friedman, K. (1972). A Regenerative Calcium Response in Paramecium. *Journal of Experimental Biology*, 56(3):667–681.

Naitoh, Y. and Kaneko, H. (1972). Reactivated Triton-Extracted Models of Paramecium: Modification of Ciliary Movement by Calcium Ions. *Science*, 176(4034):523–524.

Nakada, C., Ritchie, K., Oba, Y., Nakamura, M., Hotta, Y., Iino, R., Kasai, R. S., Yamaguchi, K., Fujiwara, T., and Kusumi, A. (2003). Accumulation of anchored proteins forms membrane diffusion barriers during neuronal polarization. *Nature Cell Biology*, 5(7):626–632.

Narahashi, T., Moore, J. W., and Scott, W. R. (1964). Tetrodotoxin Blockage of Sodium Conductance Increase in Lobster Giant Axons. *The Journal of General Physiology*, 47(5):965–974.

Naundorf, B., Wolf, F., and Volgushev, M. (2006). Unique features of action potential initiation in cortical neurons. *Nature*, 440(7087):1060–1063.

Neher, E. and Sakmann, B. (1976). Single-channel currents recorded from membrane of denervated frog muscle fibres. *Nature*, 260(5554):799–802.

Oertel, D., Schein, S. J., and Kung, C. (1977). Separation of membrane currents using a Paramecium mutant. *Nature*, 268(5616):120–124.

Ogura, A. and Takahashi, K. (1976). Artificial deciliation causes loss of calcium-dependent responses in Paramecium. *Nature*, 264(5582):170–172.

Overton, E. (1902). Beitrge zur allgemeinen Muskel- und Nervenphysiologie. *Archiv fr die gesamte Physiologie des Menschen und der Tiere*, 92(3-5):115–280.

Palmer, L. M. and Stuart, G. J. (2006). Site of action potential initiation in layer 5 pyramidal neurons. *J Neurosci*, 26(6):1854–1863.

Patlak, J. (1991). Molecular kinetics of voltage-dependent Na+ channels. *Physiological Reviews*, 71(4):1047–1080.

Perge, J. A., Niven, J. E., Mugnaini, E., Balasubramanian, V., and Sterling, P. (2012). Why Do Axons Differ in Caliber? *The Journal of Neuroscience*, 32(2):626–638.

Peters, A. (1968). THE SMALL PYRAMIDAL NEURON OF THE RAT CEREBRAL CORTEX: The Axon Hillock and Initial Segment. *The Journal of Cell Biology*, 39(3):604–619.

Peterson, B. Z., DeMaria, C. D., and Yue, D. T. (1999). Calmodulin Is the Ca2+ Sensor for Ca2+-Dependent Inactivation of L-Type Calcium Channels. *Neuron*, 22(3):549–558.

Phillips, R., Kondev, J., and Theriot, J. (2008). *Physical Biology of the Cell*. Garland Science, New York, 1 edition edition.

Pineda, R. H. and Ribera, A. B. (2007). Evolution of the Action Potential. In Kaas, J. H., editor, *Evolution of Nervous Systems*, pages 211–238. Academic Press, Oxford.

Platkiewicz, J. and Brette, R. (2010). A threshold equation for action potential initiation. *PLoS Computational Biology*, 6(7):e1000850.

Popper, K. R. (1959). *The logic of scientific discovery*. Basic Books, Oxford, England.

Purves, R. D. (1981). *Microelectrode methods for intracellular recording and ionophoresis*. Academic Press New York.

Puthussery, T., Venkataramani, S., Gayet-Primo, J., Smith, R. G., and Taylor, W. R. (2013). NaV1.1 channels in axon initial segments of bipolar cells augment input to magnocellular visual pathways in the primate retina. *The Journal of Neuroscience: The Official Journal of the Society for Neuroscience*, 33(41):16045–16059.

Rall, W. (1969). Time Constants and Electrotonic Length of Membrane Cylinders and Neurons. *Biophysical Journal*, 9(12):1483–1508.

Rall, W. (2011). Core Conductor Theory and Cable Properties of Neurons. In *Comprehensive Physiology*. John Wiley & Sons, Inc.

Ramon-y Cajal, S. (1899). *Texture of the Nervous System of Man and the Vertebrates*.

Roberts, A. and Mackie, G. O. (1980). The giant axon escape system of a hydrozoan medusa, Aglantha digitale. *The Journal of Experimental Biology*, 84:303–318.

Rosen, R. (1985). *Anticipatory Systems: Philosophical, Mathematical and Methodological Foundations*. Pergamon Pr, Oxford u.a., 1st edition edition.

Rosker, C., Lohberger, B., Hofer, D., Steinecker, B., Quasthoff, S., and Schreibmayer, W. (2007). The TTX metabolite 4,9-anhydro-TTX is a highly specific blocker of the Na(v1.6) voltage-dependent sodium channel. *American Journal of Physiology. Cell Physiology*, 293(2):C783–789.

Rossant, C., Goodman, D. F. M., Fontaine, B., Platkiewicz, J., Magnusson, A. K., and Brette, R. (2011). Fitting neuron models to spike trains. *Frontiers in Neuroscience*, 5:9.

Rossant, C., Goodman, D. F. M., Platkiewicz, J., and Brette, R. (2010). Automatic fitting of spiking neuron models to electrophysiological recordings. *Frontiers in Neuroinformatics*, 4:2.

Rush, A. M., Dib-Hajj, S. D., and Waxman, S. G. (2005). Electrophysiological properties of two axonal sodium channels, Nav1.2 and Nav1.6, expressed in mouse spinal sensory neurones. *The Journal of Physiology*, 564(3):803–815.

Saimi, Y. and Kung, C. (1987). Behavioral genetics of Paramecium. *Annual Review of Genetics*, 21:47–65.

Saimi, Y. and Kung, C. (1994). Ion channel regulation by calmodulin binding. *FEBS Letters*, 350(2):155–158.

Satow, Y. (1978). Internal calcium concentration and potassium permeability in Paramecium. *Journal of Neurobiology*, 9(1):81–91.

Satow, Y. and Kung, C. (1976). A TEA+-insensitive mutant with increased potassium conductance in Paramecium aurelia. *Journal of Experimental Biology*, 65(1):51–63.

Satow, Y. and Kung, C. (1980). Ca-Induced K+-Outward Current in Paramecium Tetraurelia. *Journal of Experimental Biology*, 88(1):293–304.

Scheuer, T. (2011). Regulation of sodium channel activity by phosphorylation. *Seminars in Cell & Developmental Biology*, 22(2):160–165.

Schmidt-Hieber, C. and Bischofberger, J. (2010). Fast Sodium Channel Gating Supports Localized and Efficient Axonal Action Potential Initiation. *Journal of Neuroscience*, 30(30):10233–10242.

Schuetze, S. M. (1983). The discovery of the action potential. *Trends in Neurosciences*, 6:164–168.

Scott, L. L., Mathews, P. J., and Golding, N. L. (2005). Posthearing Developmental Refinement of Temporal Processing in Principal Neurons of the Medial Superior Olive. *The Journal of Neuroscience*, 25(35):7887–7895.

Sekerli, M., Del Negro, C. A., Lee, R. H., and Butera, R. J. (2004). Estimating action potential thresholds from neuronal time-series: new metrics and evaluation of methodologies. *IEEE transactions on bio-medical engineering*, 51(9):1665–1672.

Sengupta, B., Stemmler, M., Laughlin, S. B., and Niven, J. E. (2010). Action Potential Energy Efficiency Varies Among Neuron Types in Vertebrates and Invertebrates. *PLOS Computational Biology*, 6(7):e1000840.

Seyfarth, E.-A. (2006). Julius Bernstein (1839-1917): pioneer neurobiologist and biophysicist. *Biological Cybernetics*, 94(1):2–8.

Sibaoka, T. (1962). Excitable cells in Mimosa. *Science (New York, N.Y.)*, 137(3525):226.

Sigworth, F. J. and Neher, E. (1980). Single Na channel currents observed in cultured rat muscle cells. *Nature*, 287(2):447.

Singer, S. J. and Nicolson, G. L. (1972). The Fluid Mosaic Model of the Structure of Cell Membranes. *Science*, 175(4023):720–731.

Slayman, C. L., Scott Long, W., and Gradmann, D. (1976). Action potentials in NEUROSPORA CRASSA, a mycelial fungus. *Biochimica et Biophysica Acta (BBA) - Biomembranes*, 426(4):732–744.

Sloper, J. J. and Powell, T. P. S. (1979). A Study of the Axon Initial Segment and Proximal Axon of Neurons in the Primate Motor and Somatic Sensory Cortices. *Philosophical Transactions of the Royal Society of London. Series B, Biological Sciences*, 285(1006):173–197.

Stuart, G., Spruston, N., Sakmann, B., and Hausser, M. (1997). Action potential initiation and backpropagation in neurons of the mammalian CNS. *Trends Neurosci*, 20(3):125. undefined Action potential initiation and backpropagation in neurons of the mammalian CNS 615 97215514 0166-2236 Journal Article Review Review, Academic NOT IN FILE http://www.ncbi.nlm.nih.gov/entrez/query.fcgi?cmd=Retrieve&db=PubMed&dopt=Citation&list_uids=906 Division of Neuroscience, John Curtin School of Medical Research, Australian National University, Canberra, Australia.

Stuart, G. J. and Sakmann, B. (1994). Active propagation of somatic action potentials into neocortical pyramidal cell dendrites. *Nature*, 367(6458):69–72.

Tasaki, I. (2012). *Physiology and Electrochemistry of Nerve Fibers*. Elsevier.

Tasaki, I., Nakaye, T., and Byrne, P. M. (1985). Rapid swelling of neurons during synaptic transmission in the bullfrog sympathetic ganglion. *Brain Research*, 331(2):363–365.

Tauc, L. (1962). Site of Origin and Propagation of Spike in the Giant Neuron of Aplysia. *The Journal of General Physiology*, 45(6):1077–1097.

Taylor, A. R. (2009). A Fast Na+/Ca2+-Based Action Potential in a Marine Diatom. *PLoS ONE*, 4(3):e4966.

Tchumatchenko, T., Malyshev, A., Wolf, F., and Volgushev, M. (2011). Ultrafast population encoding by cortical neurons. *The Journal of Neuroscience: The Official Journal of the Society for Neuroscience*, 31(34):12171–12179.

Telenczuk, M., Fontaine, B., and Brette, R. (2017). The basis of sharp spike onset in standard biophysical models. *PLOS ONE*, 12(4):e0175362.

ten Tusscher, K. H. W. J., Noble, D., Noble, P. J., and Panfilov, A. V. (2004). A model for human ventricular tissue. *American Journal of Physiology. Heart and Circulatory Physiology*, 286(4):H1573–1589.

Testa-Silva, G., Verhoog, M. B., Linaro, D., de Kock, C. P. J., Baayen, J. C., Meredith, R. M., De Zeeuw, C. I., Giugliano, M., and Mansvelder, H. D. (2014). High Bandwidth Synaptic Communication and Frequency Tracking in Human Neocortex. *PLoS Biol*, 12(11):e1002007.

Thomas, R. C. (2009). The plasma membrane calcium ATPase (PMCA) of neurones is electroneutral and exchanges 2 H+ for each Ca2+ or Ba2+ ion extruded. *The Journal of Physiology*, 587(2):315–327.

Thome, C., Kelly, T., Yanez, A., Schultz, C., Engelhardt, M., Cambridge, S., Both, M., Draguhn, A., Beck, H., and Egorov, A. (2014). Axon-Carrying Dendrites Convey Privileged Synaptic Input in Hippocampal Neurons. *Neuron*, 83(6):1418–1430.

Trunova, S., Baek, B., and Giniger, E. (2011). Cdk5 Regulates the Size of an Axon Initial Segment-Like Compartment in Mushroom Body Neurons of the Drosophila Central Brain. *The Journal of Neuroscience*, 31(29):10451–10462.

Tuckwell, H. (1988a). *Introduction to theoretical neurobiology, vol 1: linear cable theory and dendritic structure*. Cambridge University Press, Cambridge. undefined Introduction to theoretical neurobiology, vol 1: linear cable theory and dendritic structure 3 NOT IN FILE.

Tuckwell, H. (1988b). *Introduction to theoretical neurobiology, vol 2: nonlinear and stochastic theories*. Cambridge University Press, Cambridge. undefined Introduction to theoretical neurobiology, vol 2: nonlinear and stochastic theories 192 NOT IN FILE.

Umrath, K. (1930). Untersuchungen ber Plasma und Plasmastrmung an Characeen. *Protoplasma*, 9(1):576–597.

Undrovinas, A. I., Fleidervish, I. A., and Makielski, J. C. (1992). Inward sodium current at resting potentials in single cardiac myocytes induced by the ischemic metabolite lysophosphatidylcholine. *Circulation research*, 71(5):1231–1241.

Van Wart, A., Trimmer, J. S., and Matthews, G. (2007). Polarized distribution of ion channels within microdomains of the axon initial segment. *The Journal of Comparative Neurology*, 500(2):339–352.

Vandenberg, C. A. and Bezanilla, F. (1991a). Single-channel, macroscopic, and gating currents from sodium channels in the squid giant axon. *Biophysical Journal*, 60(6):1499–1510.

Vandenberg, C. A. and Bezanilla, F. (1991b). A sodium channel gating model based on single channel, macroscopic ionic, and gating currents in the squid giant axon. *Biophysical Journal*, 60(6):1511–1533.

Verkhratsky, A., Krishtal, O., and Petersen, O. (2006). From Galvani to patch clamp: the development of electrophysiology. *Pflgers Archiv European Journal of Physiology*, 453(3):233–247.

Verkman, A. S. (2002). Solute and macromolecule diffusion in cellular aqueous compartments. *Trends in Biochemical Sciences*, 27(1):27–33.

Wayne, R. (1994). The excitability of plant cells: With a special emphasis on characean internodal cells. *The Botanical Review*, 60(3):265–367.

Whittaker, E. T. E. T. (1910). *A history of the theories of aether and electricity : from the age of Descartes to the close of the nineteenth century*. London ; New York : Longmans, Green [etc., etc.].

Wilent, W. B. and Contreras, D. (2005). Stimulus-dependent changes in spike threshold enhance feature selectivity in rat barrel cortex neurons. *J Neurosci*, 25(11):2983–91. undefined Mar 16 Stimulus-dependent changes in spike threshold enhance feature selectivity in rat barrel cortex neurons 15772358 1529-2401 Journal Article http://www.ncbi.nlm.nih.gov/entrez/query.fcgi?cmd=Retrieve&db=PubMed&dopt=Citation&list_uids=157 Department of Neuroscience, University of Pennsylvania School of Medicine, Philadelphia, Pennsylvania 19106-6074, USA.

Wittmack, E. K., Rush, A. M., Hudmon, A., Waxman, S. G., and Dib-Hajj, S. D. (2005). Voltage-Gated Sodium Channel Nav1.6 Is Modulated by p38 Mitogen-Activated Protein Kinase. *Journal of Neuroscience*, 25(28):6621–6630.

Wollner, D. A. and Catterall, W. A. (1986). Localization of sodium channels in axon hillocks and initial segments of retinal ganglion cells. *Proceedings of the National Academy of Sciences*, 83(21):8424–8428.

Wyatt, K. D., Tanapat, P., and Wang, S. S.-H. (2005). Speed limits in the cerebellum: constraints from myelinated and unmyelinated parallel fibers. *The European journal of neuroscience*, 21(8):2285–2290.

Xu, K., Zhong, G., and Zhuang, X. (2013). Actin, Spectrin, and Associated Proteins Form a Periodic Cytoskeletal Structure in Axons. *Science*, 339(6118):452–456.

Young, J. Z. (1936). The Structure of Nerve Fibres in Cephalopods and Crustacea. *Proceedings of the Royal Society of London B: Biological Sciences*, 121(823):319–337.

Yu, Y., Shu, Y., and McCormick, D. A. (2008). Cortical action potential backpropagation explains spike threshold variability and rapid-onset kinetics. *The Journal of Neuroscience*, 28:7260–7272.

Zavodnik, I. B., Piasecka, A., Szosland, K., and Bryszewska, M. (1997). Human red blood cell membrane potential and fluidity in glucose solutions. *Scandinavian Journal of Clinical and Laboratory Investigation*, 57(1):59–63.

z, P., Huang, M., and Wolf, F. (2015). Action potential initiation in a multi-compartmental model with cooperatively gating Na channels in the axon initial segment. *Journal of Computational Neuroscience*, pages 1–13.

List of Figures

Index